

PRESSURE AND TEMPERATURE MEASUREMENT  
TECHNIQUES IN ELASTOHYDRODYNAMIC CONTACTS

A THESIS

Presented to

The Faculty of the Division of Graduate  
Studies and Research

By

Valentin Alexandru Turchina

In Partial Fulfillment  
of the Requirements for the Degree  
Master of Science in Mechanical Engineering

Georgia Institute of Technology

June, 1973

PRESSURE AND TEMPERATURE MEASUREMENT  
TECHNIQUES IN ELASTOHYDRODYNAMIC CONTACTS

Approved:

\_\_\_\_\_  
Ward O. Winer, Chairman

*David M. Sanborn*  
\_\_\_\_\_  
David M. Sanborn

*John L. Lundberg*  
\_\_\_\_\_  
John L. Lundberg

Date approved by Chairman: 28 May 73

#### ACKNOWLEDGMENTS

I wish to express my sincere appreciation to my advisor, Dr. Ward O. Winer for suggesting the topic of this research. Without his guidance, encouragement, and patience, this thesis could not have been completed. I would also like to thank Dr. Davis M. Sanborn for his permanent help during all stages of this research, and Dr. John Lundberg for his careful review of the manuscript.

In addition, I am indebted to all these professors for the excellent class-room teaching received from them.

Finally, I wish to acknowledge the support of NASA Grant NGR 11-002-133 and the encouragement of Mr. R. L. Johnson of NASA-Lewis in connection with this research.

## TABLE OF CONTENTS

	Page
ACKNOWLEDGMENTS . . . . .	i
LIST OF TABLES . . . . .	iii
LIST OF FIGURES . . . . .	iv
NOMENCLATURE . . . . .	v
SUMMARY . . . . .	vi
Chapter	
I. INTRODUCTION . . . . .	1
II. PRESSURE DISTRIBUTION MEASUREMENTS	
Background . . . . .	3
History of the Experimental Work. . . . .	4
Description of the Experimental Technique . . . . .	6
Discussion and Conclusions. . . . .	13
Recommendations . . . . .	14
III. TEMPERATURE DISTRIBUTION MEASUREMENTS	
Background . . . . .	16
Experimental Background . . . . .	18
Experimental Equipment and Technique. . . . .	19
Experimental Results. . . . .	36
Discussion of Results . . . . .	41
Conclusions . . . . .	46
IV. APPENDICES . . . . .	60
V. REFERENCES . . . . .	62

LIST OF TABLES

Table	Page
1. Experimental Data for Speed of 1.39 m/sec (54.9 in/sec) and Load of 6.8 Kgf (15 lbf) . . . . .	49
2. Experimental Data for Speed of 0.69 m/sec (27.4 in/sec) and Load of 6.8 Kgf (15 lbf) . . . . .	58
3. Experimental Data for Speed of 0.35 m/sec (13.7 in/sec) and Load of 6.8 Kgf (15 lbf) . . . . .	59

## LIST OF FIGURES

Figure	Page
1. Schematic Diagram of the Experimental Apparatus for Pressure Measurement . . . . .	7
2. Geometry of the Bearing Sapphire . . . . .	8
3. Detail of the Needle - Sapphire Assembly. . . . .	9
4. Needle - Sapphire Assembly Used for Pressure Calibration . . . . .	11
5. Calibration Curve for the Pressure Transducer . . . . .	12
6. Schematic Diagram of the Experimental Equipment . . . . .	20
7. Radiance Incident on the Detector (Angles Exaggerated for Clarity) . . . . .	22
8. Oil Film Filter (Not to Scale) . . . . .	31
9. Steady State Film Temperature in the EHD Contact at 1.39 m/sec (54.9 ips) Sliding Speed. . . . .	34
10. Ball Surface Temperature in the EHD Contact at 1.39 m/sec (54.9 ips) Sliding Speed . . . . .	35
11. Interference Fringe Pattern of the EHD Contact at 1.39 m/sec (54.9 ips) Sliding Speed. . . . .	37
12. Steady State Film Temperature Distribution along the Contact Centerline as a Function of Sliding Speed . . . . .	39
13. Ball Surface Temperature along the Contact Centerline as a Function of Sliding Speed . . . . .	40
14. Maximum Ball Surface Temperature and Film Temperature as a Function of Sliding Speed . . . . .	42
15. Contact Region with External Heat Source (Asperity Contacts) . . . . .	47

## NOMENCLATURE

- E - microscope output signal - volts  
f - traction force - N  
h - film thickness - m  
k - instrument constant  
n - radiance watts/cm<sup>2</sup> - steradian  
N<sup>BB</sup> - black body radiance  
N<sub>o</sub> - black body radiance at ambient temperature  
T - temperature - C  
t - transmissivity  
U - sliding velocity - m/s  
α - absorptivity  
α\* - pressure viscosity coefficient - m<sup>2</sup>/N  
ε - emissivity  
η - an attenuation factor  
ρ - reflectivity

## subscripts

- b - steel ball  
b1 - steel ball of emissivity 0.28  
b2 - steel ball of emissivity 0.47  
F - Filter  
f - EHD oil film  
s - sapphire

## SUMMARY

This research concerns the development of techniques to measure two parameters in elastohydrodynamic point contact lubrication. The measurement of lubrication parameters of pressure distribution, and temperature distribution for the very severe conditions of the contact can be an important tool in the design of the machine parts and in selecting the most efficient lubricant for them.

The object of the research performed was to investigate the feasibility of both a proposed pressure measurement technique and a temperature measurement technique.

The pressure measurement technique employed a transducer which consists of a  $9.0 \times 10^{-5}$  m (.0035 in.) diameter piston attached to a cantilever load cell and allowed to move in a  $9.0 \times 10^{-5}$  diameter orifice in the sapphire bearing plate.

The temperature measurement system consists of an infrared micro-detector used to collect infrared radiant energy from the elastohydrodynamic contact and, thereby, allowing the deduction of the local temperature. The problem of separating the infrared radiance contributions from the ball, lubricant film and sapphire bearing plate has been solved by collecting the infrared radiation under these different conditions, two of them using steel spheres with different emissivities and, one using a filter consisting of a calibrated

fluid sample "cell", placed between the infrared detector and sapphire bearing plate.

The research was entirely experimental in nature and, in each of the above two measurement systems (pressure and temperature) this thesis has the objective of simply showing the feasibility of the techniques. Therefore, the number of fluids examined and operating conditions used were limited.

## CHAPTER I

### INTRODUCTION

The theoretical and experimental study of elastohydrodynamic lubrication has a relatively short history. Elastohydrodynamic lubrication is the study of situations where the elastic deformation of the machine components plays a significant role in the hydrodynamic lubrication process.

Most of the moving machine components undoubtedly work with large bearing areas, but for small parts such as ball bearings or gears, these areas decrease in size approaching line or point contact. The conditions in such contacts are much more severe, the local pressures are high, the film thickness is very small and the viscosity increases very much because of high pressures.

The most used classification in lubrication field with respect to contact conditions are known as:

- Martin's conditions : rigid solids, isoviscous lubricant.
- Hertzian conditions : dry contact, elastic solids.
- Elastohydrodynamic conditions : elastic solids, Newtonian lubricant.

The diameter of Hertzian zone of contact which also represents the region of hydrodynamic pressure generation in the elastohydrodynamic contact is often in vicinity of  $2.54 \times 10^{-4}$  m ( $10^{-2}$  in). Theoretical results, verified in experimental investigations, show a film thickness

in such contacts as low as  $2.54 \times 10^{-8}$  m ( $10^{-6}$  in). The surface speeds of the machine components forming elastohydrodynamic contacts are usually in range of 0.254 - 25.4 m/sec (10 - 1000 ips). The average time required for the fluid to pass through such contacts is  $10^{-4}$  or  $10^{-5}$  sec. The local pressures to which the lubricant is subjected are as high as  $0.69 - 1.38 \times 10^9$  N/m<sup>2</sup> (100 - 200 kpsi), resulting in a normal stress distribution in the contact area which may produce local elastic deformations which can be significant when compared to the lubricant film thickness.

The temperature rise within the elastohydrodynamic contact area has two important influences. One on the surfaces of the machine components which will be subject to a high rate of temperature variation. The second influence will be on the fluid properties, such as viscosity, while passing through the contact area.

Because of the elevated temperature to which the contact area is subjected the thermal properties of the lubricant and bearing material are considered an important influence on the failure of highly-loaded lubricated contacts. The knowledge from research in this field of EHD is already being used by design engineers [1,2].

## CHAPTER II

### PRESSURE DISTRIBUTION MEASUREMENTS

#### Background

The early theory related to pressure distribution employing low loads or high speeds shows that the distribution reaches relatively low values as described by Martin [3]. When the load increases, or the speeds are reduced, the pressure distribution changes from Martin's form toward a Hertzian profile [4].

Elastohydrodynamic theory for a Newtonian lubricant predicts a rather spectacular disturbance to the limiting semielliptical pressure distribution in the form of a sharp pressure peak near the outlet end of the contact [5].

The initial solutions of Dawson and Higginson [6] failed to predict pressure spikes, but the theoretical work of Grubin [7] has predicted such pressure spikes in Newtonian fluids.

The distribution of pressure in EHD conditions is of great current interest because this is an area of investigations in which experiment and theory are not entirely in accord.

Pressure distributions over the contact area are of particular interest because of their effect on fatigue failure which results in small particles of material breaking out of the surfaces of gears,

bearings, cams, and other members subjected to repeated stressing action. These failures are variously known as pitting, spalling, shelling, etc. For point contacts the maximum shear stress in the solid is about one third of local pressure magnitude and it occurs at a depth of about half the radius of the contact surface [8]. In addition, instantaneous local temperatures at the point contact may be of the order of 500°F above ambient\*, generating important thermal stresses in addition to the existing shear stresses and the resulting increase in maximum contact-zone stresses may be appreciable.

#### History of the Experimental Work

A literature search of the problem did not reveal many successful techniques to determine the pressure distribution across the elastohydrodynamic contact. G. Nieman and F. Gartner [9] performed a direct measurement of the hydrodynamic pressure distribution at line contacts. The extent of pressure distribution perpendicular to the line contact is on the order of the Hertzian width, from  $2.03 \times 10^{-4}$  m (.008 in) to  $6.1 \times 10^{-4}$  m (.025 in). Their equipment consisted of rotating a flat steel disc loaded against a stationary steel cylinder. The steel cylinder has a small orifice which allows the lubricant to pass from the elastohydrodynamic contact to a strain gage pressure transducer. One of the problems which arose was machining the extremely small orifice required for the pressure measurement.

---

\*See Chapter III of this thesis.

The pressure distribution profile from Nieman and Gartner [9] experiment is not in agreement with the theoretical pressure distribution [7]. The authors could not detect a secondary pressure peak. The failure to register a secondary peak in the pressure profile can be a result of the orifice being too large compared with the area over which this secondary pressure peak is expected.

Kannel, Bell and Allen [10] developed a pressure sensing system in which a thin film of manganin is deposited on an insulated disc. The method resulted in pressure profiles for relatively light loads and the results resemble the form of solution predicted by Martin [3] for rigid cylinders. There was no evidence of the secondary pressure spike predicted by elastohydrodynamic theory for a Newtonian fluid.

Hamilton and Moore [4] have determined pressure profiles along with film thickness and temperature distribution on a four disc machine. The machine has two lower discs and one upper disc supporting between them a fourth disc made of glass. This disc is supported entirely by the other three. Pressure gages, made of manganin whose electrical resistance is sensitive to pressure were evaporated on the surface of the glass disc. Their results failed to correspond with the theory [7] in that the pressure spike was less than predicted by theory. This failure can be explained by the fact that the authors employed a transducer with a relatively low resolving power, resulting in the pressure being averaged over the relatively large surface of the gage.

### Description of the Experimental Technique

The equipment (Figure 1) that was employed to determine the pressure distribution in elastohydrodynamic point contact lubrication is basically the same as that used in Reference [11,12]. The spherical bearing surface is a steel ball of  $3.18 \times 10^{-2}$  m (1.25 in) diameter. The sphere is rotated through a flexible coupling cemented to its surface. The sphere is supported and loaded against the bearing sapphire by three radial ball bearings of dimensions similar to the rotating sphere and located in a lubricated bath. A significant amount of inertia was incorporated into the drive mechanism in order to maintain a nearly constant sliding velocity between the spherical bearing and sapphire while the load is on and off.

The upper surface of the contact is a synthetic sapphire disc having one of its plane surfaces directed toward the contact. The modulus of elasticity of the sapphire is approximately twice that of the steel sphere, thus yielding a 25% greater equivalent modulus of elasticity of the steel-sapphire as compared to steel-steel systems, a value that is representative of most conventional bearing surfaces.

The synthetic sapphire bearing is a pure crystalline aluminum oxide,  $Al_2O_3$ , having a single rhombohedral uniaxial structure. The sapphire bearing used to determine the pressure distribution has the dimensions as shown in Figure 2.

The needle, designed to slide as a piston in the orifice of the sapphire, was processed from a steel rod whose end was ground in the

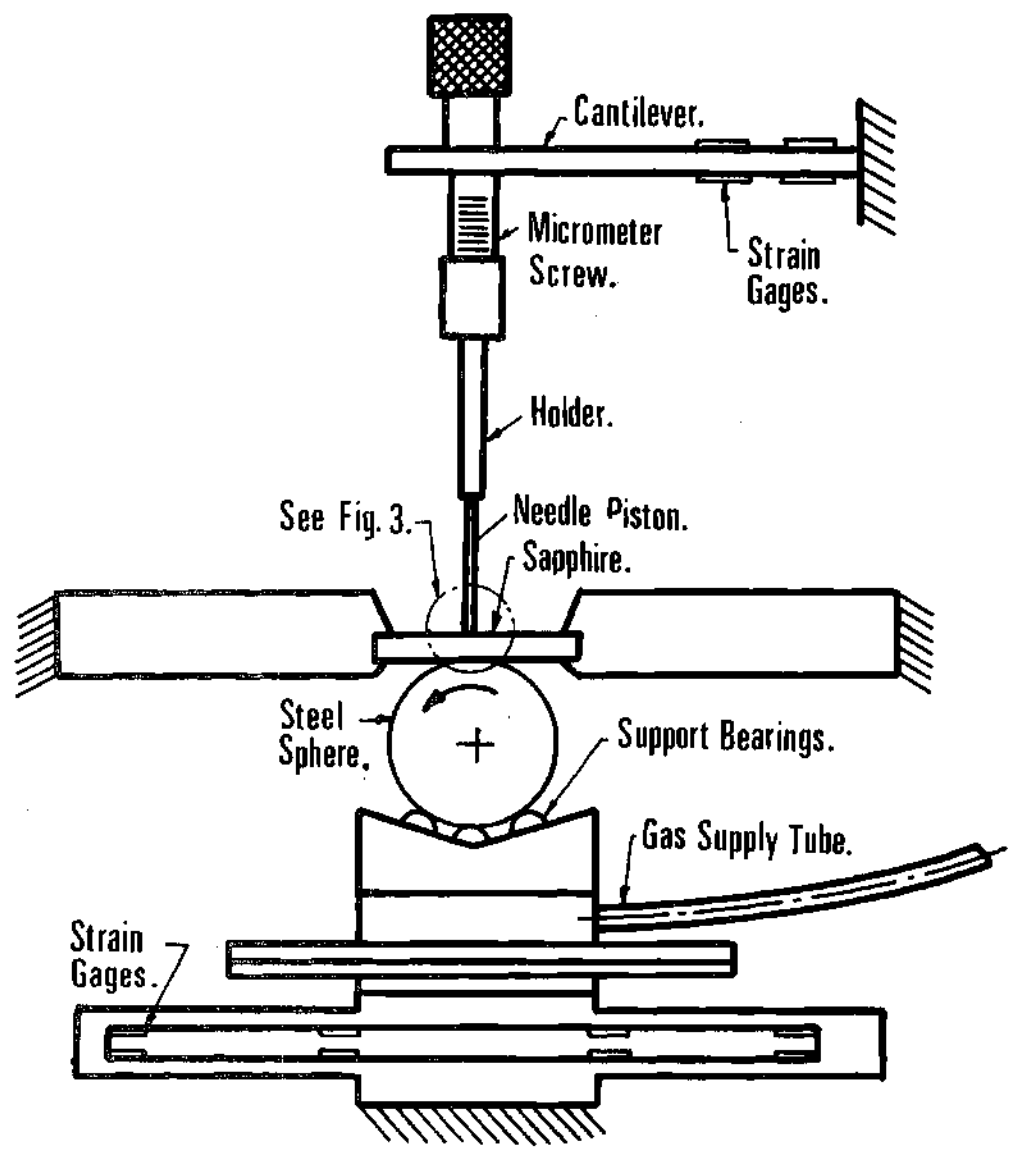


Figure 1. Schematic Diagram of the Experimental Apparatus for Pressure Measurement.

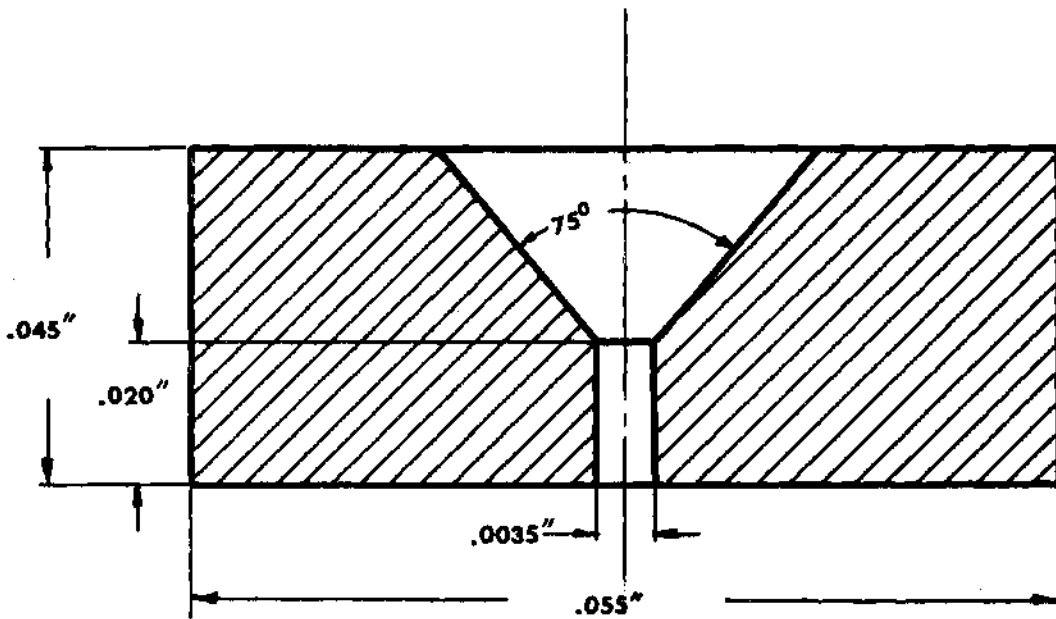


Figure 2. Geometry of the Bearing Sapphire.

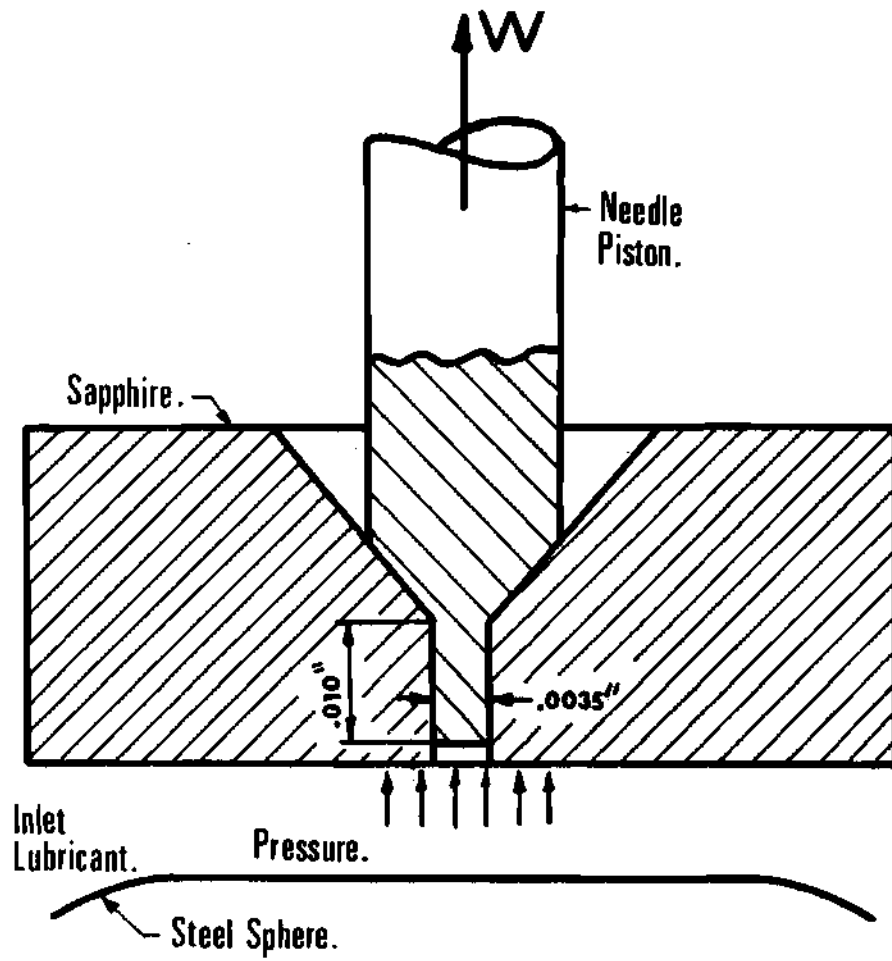


Figure 3. Detail of the Needle - Sapphire Assembly.

sapphire orifice. A diamond polishing compound with a particle size of 0.25 micron was used for grinding. The length of the needle in the sapphire was ground to  $2.504 \times 10^{-4}$  m (0.010 in) and to a corresponding diameter of  $9.0 \times 10^{-5}$  m (0.0035 in) (Figure 3). The needle was cemented to a holder rigidly attached to a micrometer screw mounted in the cantilever beam (Figure 1).

Four silicon semi-conductor strain gages were cemented on the cantilever beam. The strain gages were connected in a four gage bridge circuit and a 12 volt d.c. battery. The sensitivity of this transducer was determined to be 0.072 mV/kpsi. The maximum deflection of the cantilever beam is approximately 0.001 in/lbf.

A pneumatic system has been used to apply the normal load between the bearing surfaces. The rate of pressure rise can be controlled by restricting the flow of gas between the tanks and the bellows with an appropriate valve. In all cases nitrogen was used in the tanks at pressure less than  $2.068 \times 10^6$  N/m<sup>2</sup> (300 psi). The load transducer consists of eight foil strain gages mounted in a Wheatstone bridge circuit. The output signal of the transducer is amplified and displayed on a dual beam oscilloscope screen.

The normal force load cell was calibrated statically by placing known weights on the sphere support and recording the electrical outputs at each weight increment. A calibration curve was plotted which shows a linear response for at least 30 lbf normal load.

The transducer was calibrated in a separate mounting as shown in Figure 4. Lubricant oil at a known pressure was fed into the fitting. The pressure acting on the end of the needle resulted in a

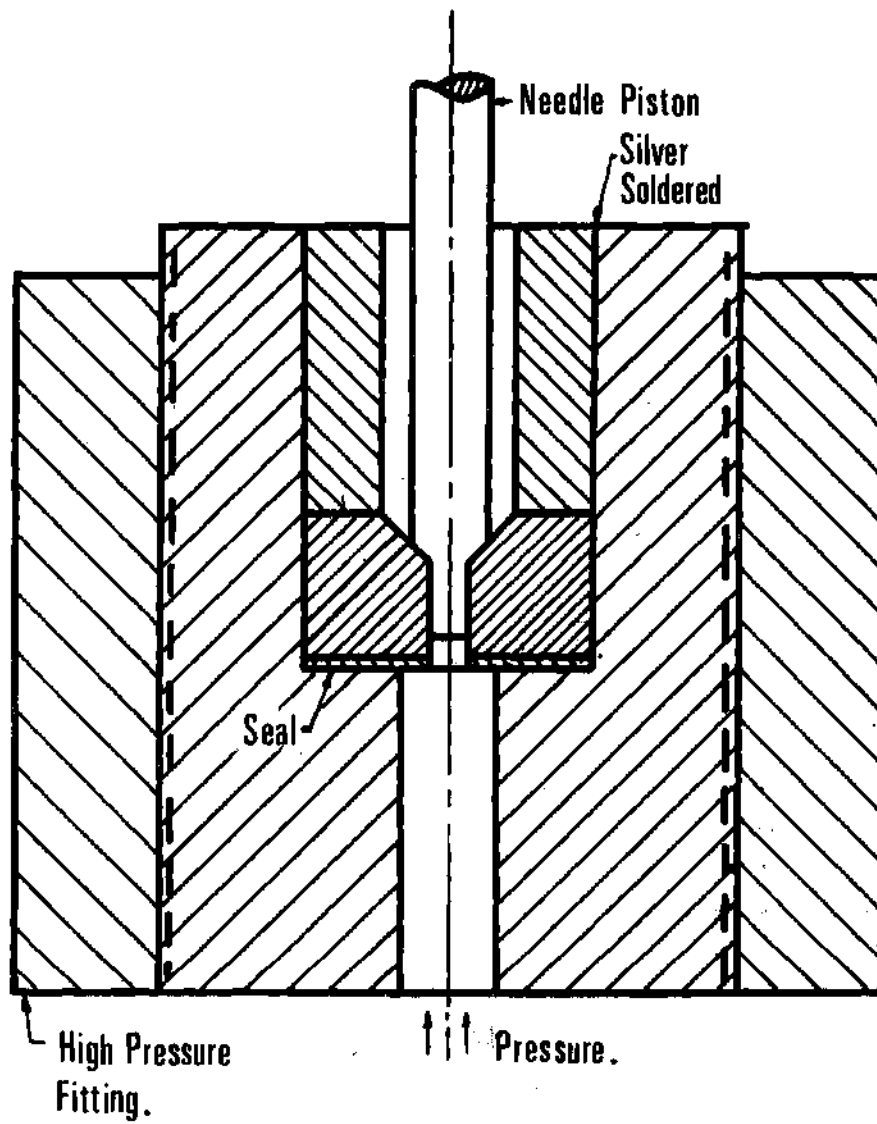


Figure 4. Needle - Sapphire Assembly Used for Pressure Calibration.

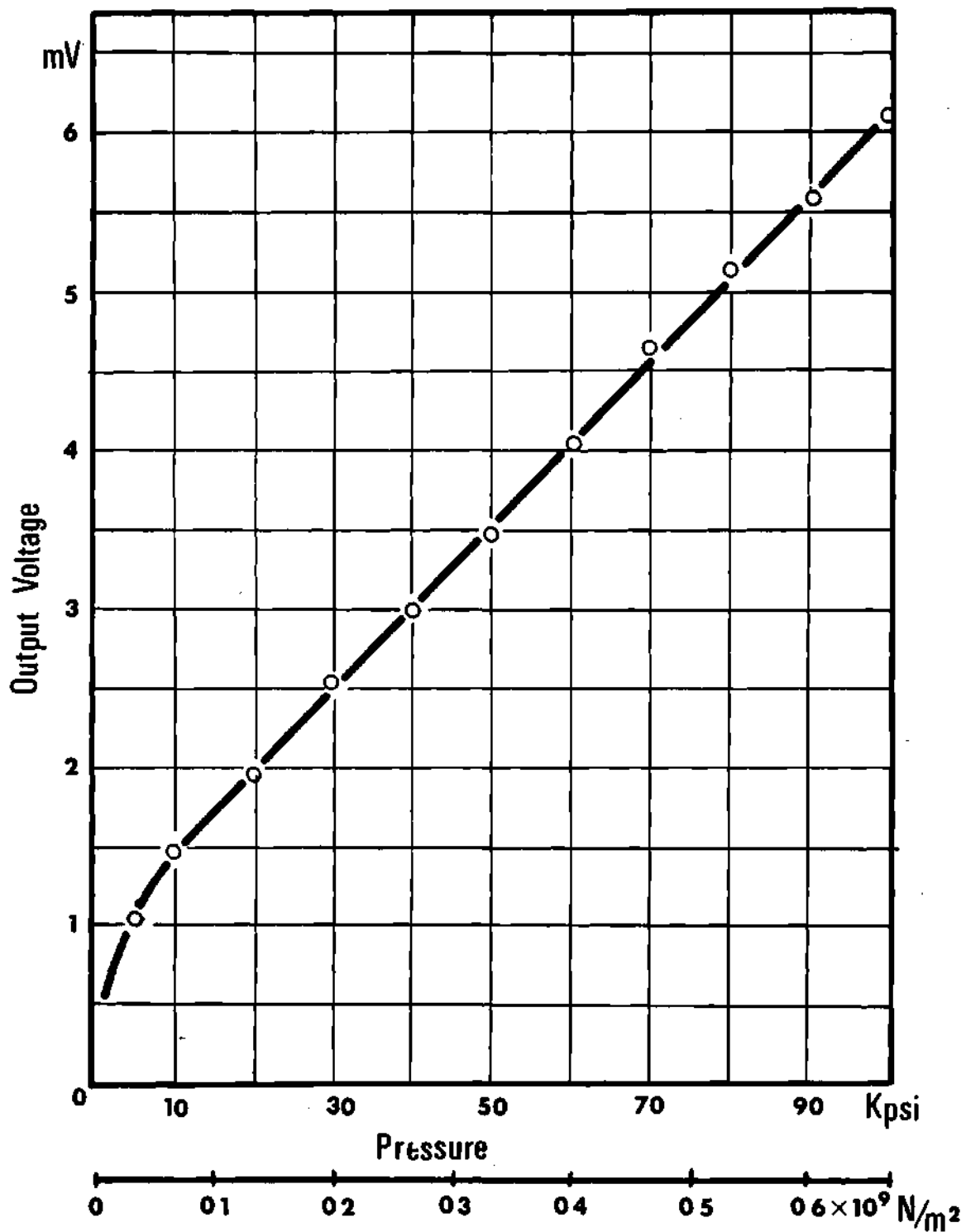


Figure 5. Calibration Curve for the Pressure Transducer.

normal force in the needle which caused a deformation in the cantilever load cell. The output voltage (see Figure 5) was plotted against each value of pressure introduced into the system  $0 - 0.69 \times 10^9 \text{ N/m}^2$  (0 - 100 kpsi). During the experiment no leakage of lubricant from the system was observed.

The location of the orifice in the sapphire bearing relative to the elastohydrodynamic contact was observed through a Leitz metallurgical microscope. The upper plate of the apparatus in which is mounted the sapphire bearing offers a two direction freedom of movement by means of micrometer screws in each direction.

#### Discussion and Conclusions

Many attempts were made to record an output signal from the transducer while passing the orifice through the elastohydrodynamic contact. None of them was successful. However, an immediate explanation of failure to record pressure could not be determined because the conditions during calibration appeared to be similar to those of an elastohydrodynamic contact.

During repeated experience a leakage of the lubricant oil between the needle and the wall of the orifice in sapphire bearing was observed, leakage that was not noticed during the calibration. The radial clearance between the needle and orifice remained the same as during calibration at a value of 0.25 micron ( $10^{-5}$  in) due to the particle size of the diamond compound used to grind the piston portion of the needle. The hydrocarbon oil used during the experiment has a viscosity of 100 cp at a pressure of  $0.69 \times 10^8 \text{ N/m}^2$  (10 kpsi). At

these conditions the leakage flow rate will be  $3.5 \times 10^{-5}$  in<sup>3</sup>/sec, for an isothermal annular flow with pressure dependent viscosity. The fluid flow rate in the elastohydrodynamic contact passing by the orifice is only  $3.0 \times 10^{-6}$  in<sup>3</sup>/sec. As the pressure builds the viscosity increases and, therefore, at very high pressures the leakage flow rate will decrease with increasing pressure. This is the case during the calibration where the fluid flow rate available was very large compared to the leakage flow rate.

Because in elastohydrodynamic conditions the "possible" leakage flow is greater than that of entering fluid flow the pressure will never build up to levels where the viscosity reaches values at which the leakage can be neglected as an important factor in pressure measurement.

An additional difficulty in the elastohydrodynamic contact is the elevated temperature which causes the viscosity to be low compared to conditions during high pressure calibration.

#### Recommendations

The technique presented in this chapter to determine a pressure profile across the elastohydrodynamic contact was found not to be feasible.

An improved machining of the needle-sapphire assembly is not recommended because the clearance between needle and orifice is already very small,  $10^{-5}$  in (.25 micron) and significantly smaller clearances are difficult to produce.

A technique employing as the upper surface bearing two sapphires

is under consideration at this time. One sapphire having a small orifice open toward elastohydrodynamic contact is topped by a second sapphire which has a manganin strain gage evaporated on its surface. The method combines two of the most widely used techniques in experimental research to determine the pressure distribution; the orifice technique and that of evaporated manganin strain gage. This method appears to solve the difficulties which were encountered in each of the separate techniques. The leakage flow rate from the piston - orifice technique is eliminated by not employing a piston and, the manganin strain gages are no longer exposed directly to the severe stress conditions of the elastohydrodynamic contact. The orifice in the sapphire can be enlarged at the upper exit allowing the use of a coil strain gage, rather than evaporated, with a higher resolving power necessary to detect any pressure spikes. For the same purpose the orifice at the lower exit can be reduced to very small dimensions  $2.54 \times 10^{-5}$  m (.001 in), thus narrowing the band on which the pressure is averaged.

## CHAPTER III

## TEMPERATURE DISTRIBUTION MEASUREMENTS

Background

The rheological behavior of the lubricant in an elastohydrodynamic contact is not only a function of the appropriate constitutive equation relating the stress and strain rate in the lubricant, but also of the thermodynamic state as defined by the pressure and temperature of the lubricant as it passes through the conjunction region. Because large amounts of mechanical energy are dissipated in the EHD film, particularly in contacts where there is some relative velocity between the surfaces, temperatures of the lubricant and the solid surfaces may be quite different from the ambient. The temperatures in the contact are important because the viscosity, which is probably the most important mechanical property of the lubricant in the contact is a strong function of temperature. The viscosity decrease with increasing temperature becomes larger at elevated pressures such as those occurring in EHD contacts. Temperature increases in the inlet region may influence the minimum film thickness whereas temperature increases in the high pressure region will influence traction and surface shear stresses. The surface stresses in turn are an important factor in bearing surface failure. Several attempts at defining a failure criterion through a thermal analysis of lubricant films have been made; the most notable of which is Blok's flash temperature theory [13]. Because of the importance of surface and film temperature in EHD films, the program described below was undertaken.

Most analytical research has assumed an isothermal fluid film thereby greatly reducing the complexity of the mathematical model dealt with. Notable exceptions to this are the works of Crook [14], Cheng and Sternlicht [15], Dowson [16], and Archard [17 & 18]. In all of these investigations it was not only necessary to assume mechanical and thermal constitutive equations for the lubricant, but also to assume thermal boundary conditions for the film. In this chapter is described a technique for measuring temperatures in the EHD contact. The technique is based on the emitted infrared radiation from the contact area. No physical probe is interjected into the conjuncture region which consists of the lubricant film between a moving steel surface and a stationary sapphire surface. IR radiation from the two solid surfaces and the lubricant film passes through the sapphire surface and is measured by a cryogenically cooled In-Sb detector. The detector can measure radiation from an area within the contact small enough to permit the mapping of contact temperatures. Through an appropriate set of measurements the radiation from the steel ball surface and the lubricant film can each be separated from the total radiation received by the detector. This permits the determination of the local steel ball surface temperature and a local lubricant temperature averaged through the film.

Because the surfaces used for the EHD contact are steel and sapphire, the pressures in the contact are in the range of current design practice. The maximum Hertz pressure is  $1.034 \times 10^9 \text{ N/m}^2$  (150,000 psi) for the data reported. These data are for a sliding contact. For a given set of conditions the ball surface temperature reaches a maximum of  $115^\circ\text{C}$  and average fluid temperature reaches a maximum of  $360^\circ\text{C}$ , both occurring near the side lobes. The experiment

is performed in a room temperature environment.

This chapter is concerned primarily with reporting a technique for measuring temperatures in a EHD contact. This technique is not restricted to conditions employed in the contact for which data are reported. The procedure can also be applied to rolling contacts where the sapphire surface is moving. A technique is currently being developed which is an extension of the method described below and which will also permit the determination of the sapphire surface temperature. Because we have demonstrated that the IR emission from an EHD contact is sufficiently large that it can be measured with existing detectors, it may be possible to perform a spectral analysis of this radiation and to deduce from the spectra detailed information about the state and interactions of the materials in the contact.

The temperature distributions obtained, along with film thickness and traction data from the same apparatus can be used to evaluate lubricant constitutive equations. More important from a design point of view, the temperature distributions can be used to detect the onset of lubricant film failure and thereby evaluate or establish limiting design criteria for lubricated contacts.

#### Experimental Background

Relatively little experimental research has been directed toward the determination of temperatures in the elactohydrodynamic contact. Hamilton and Moore [4] used a nickel film gauge evaporated on a glass disc. The gauge is made from a material with a high temperature coefficient of resistivity. With it measurement of the temperature distribution over the contact area were possible. All cases investigated

by them are at low Hertz pressure conditions because a glass disc was employed. The maximum temperature was found to occur in the inlet, and the temperature variation over the rolling contact is very small ( $1^{\circ}\text{C}$ ).

Cheng and Orcutt [19] made temperature measurements for rolling contacts using a platinum film gauge on a glass disc. The temperature rise recorded by them is also very small ( $3^{\circ}\text{C}$ ) and it can be explained because of low Hertz pressure conditions over the contact, and possibly because of low resolving power of the gauges employed. Both of the techniques described above have experienced difficulties in evaporating the gauges on the disc, and both were limited to low pressures conditions imposed by the glass disc used as one of the bearing surfaces. The experiments were made more difficult by the relatively short life, either the gauges (30 min. of running with load) or the glass disc (2-3 hours of running with load).

#### Experimental Equipment and Technique

The sliding EHD point contact is formed using a  $3.18 \times 10^{-2}$  m (1.25 in) diameter steel ball rotating and loaded against a  $1.52 \times 10^{-3}$  m (0.060 in) thick sapphire flat. The system has been used previously in extensive investigations of film thickness [11], traction [12] and pressure measurement as mentioned in Chapter II.

It is shown in Figure 6, the pressure transducer has been replaced by an infrared radiometric detector (Barnes Engineering Company, Model RM-2A). The purpose of this detector is to measure the infrared radiation emitted from the contact and, therefore, allow contact temperature to be deduced.

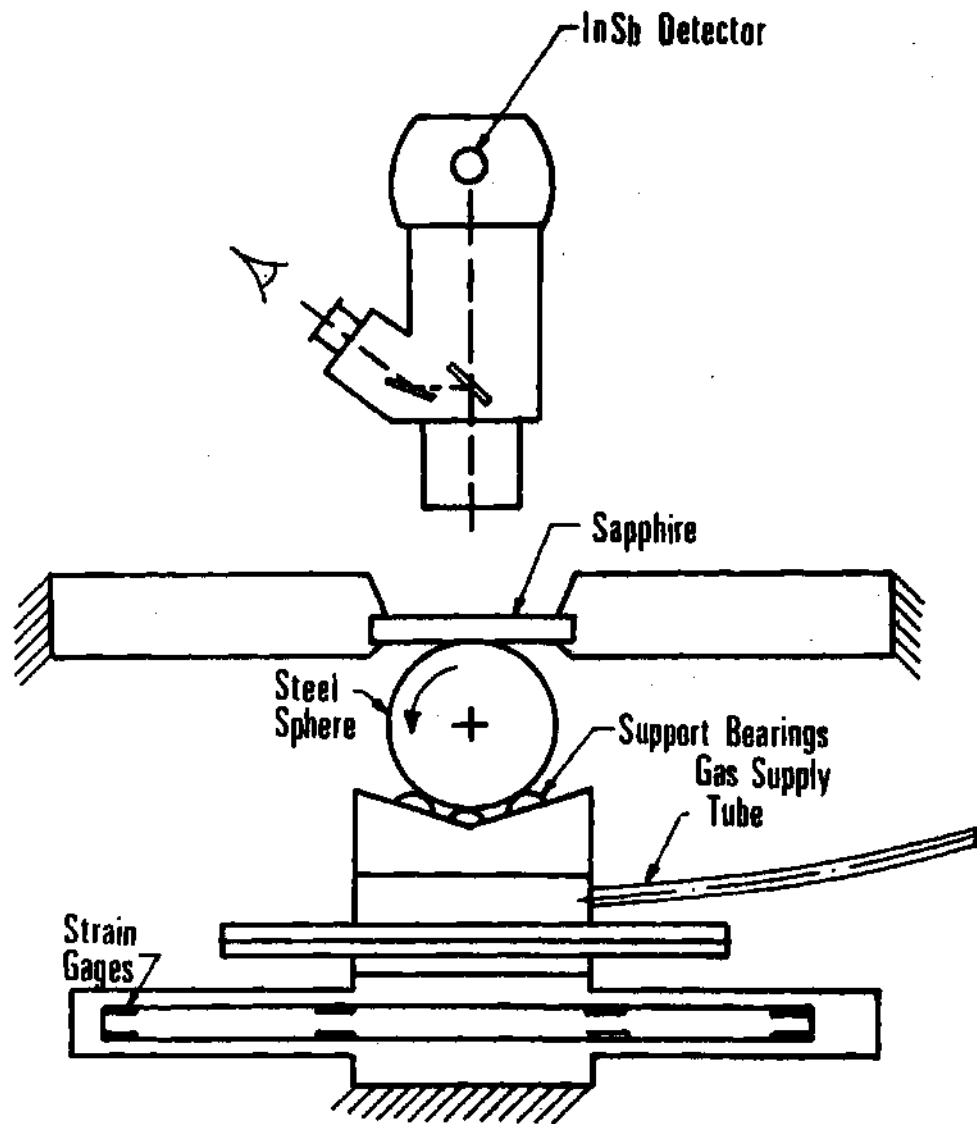


Figure 6. Schematic Diagram of the Experimental Equipment.

The radiometric detector has been equipped with a 15X reflecting objective which allows spot size resolution of  $3.56 \times 10^{-5}$  m (0.0014 in.). The radiance from this spot plus that from a related solid angle (Figure 6) between this spot and the objective, are focused onto a liquid nitrogen cooled indium antimonide detector. This detector has a spectral response of 1.8 to  $5.5 \times 10^{-6}$  m (1.8 to 5.5 microns). The sapphire has a transmissivity of 0.90 over this same range thus allowing the steel ball and oil film radiance to reach the detector. The visible light also collected by the objective is separated from the IR and is directed toward a visual eyepiece. The visual and IR systems are parfocal, and the visual field of view is twenty times as large in diameter as the area which is covered by the IR detector. The area covered by the detector is located in the center of the visual field of view and indicated by intersecting cross hairs. This allows one to focus on the oil film by visually searching for the interference fringe pattern characteristic of the EHD contact. The detector will then respond to radiance from the  $3.56 \times 10^{-5}$  m (.0014 in.) diameter oil film and steel ball surface plus a volume of the sapphire disk (see Figure 6). Since the temperatures of the lubricant film and the bearing surfaces are desired separately, rather than an average contact temperature, experimental techniques have been devised to isolate the radiance contributions from the sapphire, lubricant film, and steel ball.

Figure 7 shows the components of the radiation received by the In-Sb detector. There are four radiant sources:  $N_o$  - due to reflected ambient background radiation,  $N_s$  - due to emission from the sapphire,  $N_b$  - due to emission from the steel ball, and  $N_f$  - due to emission from the lubricant film. There is an attenuation factor associated with each

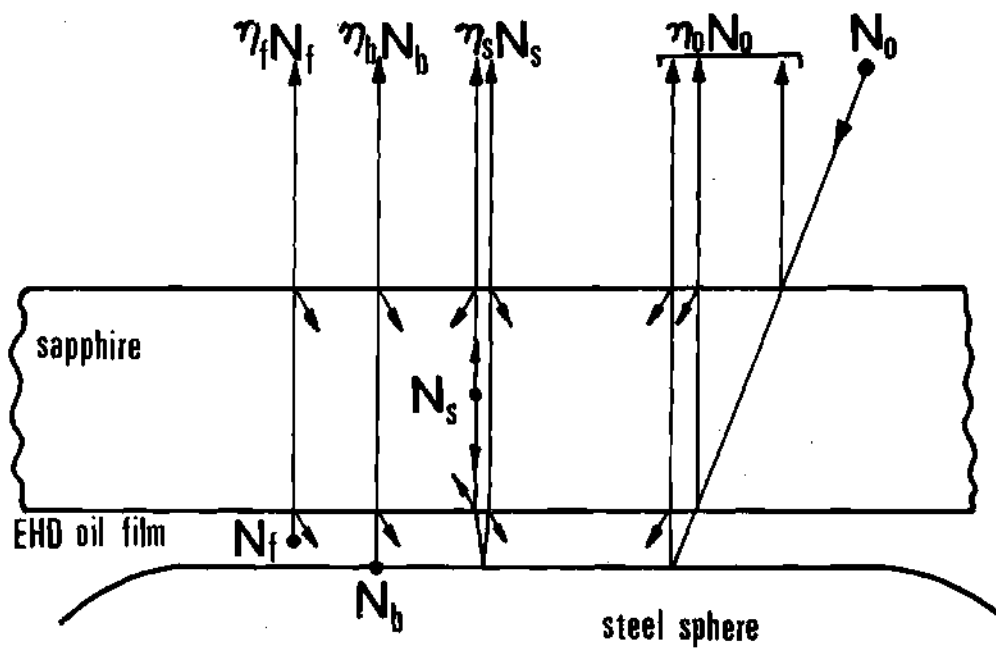


Figure 7. Radiation Incident on the Detector (Angles Exaggerated for Clarity).

of these components. Under the conditions listed below, these factors are:

$$\begin{aligned} n_o &= 0.082 + 0.683 \rho_b \\ n_s &= 1. + 0.830 \rho_b \\ n_b &= 0.830 \\ n_f &= 0.830 \end{aligned} \quad (1)$$

based on

1. Fresnel reflection losses of 0.076 at the sapphire - air interface and 0.0064 at the sapphire - oil interface [20].
2. sapphire transmissivity of 0.90 for the  $1.52 \times 10^{-3}$  m (0.060 in.) thick disk [20],
3. that the sapphire radiates to both hemispheres and a portion of the radiance initially directed toward the oil film is reflected back to the detector,
4. absorptivity of the oil film is negligible due to its thickness of approximately  $2.54 \times 10^{-7}$  m ( $10^{-5}$  in.), and
5. that, although the oil film also radiates to both hemispheres, the effect has been accounted for in the value of emissivity assigned to the film.

The IR radiometric detector contains a black body source at ambient temperature. A mechanical chopper in the detector alternately exposes the detector to the total incident radiance and then to the black body reference. The output signal, therefore, is a function of the difference between these values

$$E = k(N_{\text{TOTAL}} - N_o) \quad (2)$$

where  $k$  is known instrument constant. It can be seen from Figure 7 that the total incident radiance is given by

$$N_{\text{TOTAL}} = \eta_f N_f + \eta_b N_b + \eta_s N_s + \eta_o N_o \quad (3)$$

therefore, combining equations 1 - 3,

$$E/k = 0.830 (N_f + N_b) + (1. + 0.830 \rho_b) N_s \quad (4)$$

$$+ (0.683 \rho_b - 0.912) N_o$$

The reflectivity of the ball surface  $\rho_b$  can be measured with the radiometric detector. The quantity  $N_o$  is dependent on the ambient temperature only and can be evaluated. The individual radiance values  $N_f$ ,  $N_b$  and  $N_s$  are known functions of the source emissivity and temperature.

-3

The sapphire which is  $1.52 \times 10^{-3}$  m (0.060 in.) thick will have a large temperature gradient due to the viscous heating in the oil on one side and ambient air on the other. Radiation is emitted from throughout the thickness rather than just at a surface. Because the temperature distribution of the sapphire is unknown a sapphire surface temperature has not been determined thus far.

Since the steel ball is opaque, a surface emissivity and temperature can be associated with the radiance  $N_b$ . The emissivity of the ball surface has been determined at several temperatures using the radiometric detector. The technique is to paint a small spot of flat black paint ( $\epsilon \approx 0.95$ ) on the ball surface, heat the ball to an elevated temperature and then compare radiance values

at adjacent points on the ball surface - one on and one off the painted section. This technique gave a surface emissivity of 0.28 for the 52100 chrome steel ball. This value was reproducible at several temperature levels.

The emissivity of the oil film must be determined before a film temperature can be calculated. Since the oil film is an absorbing medium with anticipated high temperature gradients, the temperature which will be assigned to the oil film will be an average temperature across the film. Because the radiance is related to the fourth power of temperature, however, this average value will be skewed toward the maximum temperature in the film. In general, the emissivity of the oil film is a function of oil chemistry; wavelength and film thickness. The emissivity, therefore, must be determined for the lubricant being used with the same detector to be used in temperature measurements. Once the dependence on film thickness is known, film thickness profiles previously obtained [11] can be used to obtain a local emissivity value. McMahon [21] presents a relation between effective emissivity and film thickness of a semi-transparent material. For a lubricant film thickness  $h$ , considered as a heated, reflecting, partially transparent body, the relation is

$$\epsilon = \frac{(1 - \rho^*) (1 - e^{-\lambda h})}{(1 - \rho^* e^{-\lambda h})} \quad (5)$$

where  $\lambda$  is an absorption coefficient for the oil film and  $\rho^*$  is the effective reflectivity of the oil film. In a separate experiment in which a stationary ball was placed in a constant temperature

bath of the test lubricant with the sapphire resting on top of the ball, the radiance was measured near the contact between the surfaces. An oil film occupied the space between the ball and sapphire. Since the dimensions of the gap can be determined from geometry alone, the radiance data at a known fluid temperature can be transformed into a local emissivity value. The data obtained resulted in an emissivity of 0.352 for a film thickness of  $5.08 \times 10^{-5}$  m (0.002 in.). Solving equation (5) for  $\lambda$  yields  $\lambda = 9.43 \times 10^{-1}$  m (240 in.). For EHD film thicknesses on the order of  $10^{-7}$  m ( $10^{-5}$  in.), the quantity  $\lambda - h$  is of the order  $10^{-3}$ , allowing equation (5) to be accurately approximated by

$$\epsilon_f = \lambda h \quad (6)$$

For a given experiment, temperature is a function of only radiation and emissivity, therefore,

$$T_b = f(N_b, \epsilon_b) \quad (7)$$

$$T_f = f(N_f, \epsilon_f) \quad (8)$$

Since the film thickness at any point in the contact can be determined using the optical interference technique [11]  $\epsilon_b$  and  $\epsilon_f$  can be found. However, there remain three equations (4,7,8) with five unknowns ( $N_f, N_b, N_s, T_b, T_f$ ). Clearly, two additional independent relations must be found. This has been done by the following two alterations to the experiment described thus far.

In order to determine the ball surface temperature, the EHD experiment was repeated under identical conditions, but with a ball having an emissivity of 0.47 compared with that of 0.28 used in the first experiment. The increase in emissivity was accomplished by allowing the ball surface to react in a high temperature oil bath. A comparison of film thickness values taken using each ball indicated that the conditions in the contact were identical regardless of which ball was used. All other variables remaining constant, the higher ball emissivity will give a higher ball radiance  $N_b$ . The author has shown through an order of magnitude analysis (see Appendix A) that the increased radiance from the ball surface will have a negligible effect on the film and surface temperatures. Therefore, for a given point in the contact, the data from the two experiments using a low and high emissivity ball will result in two different output signals  $E_1$  and  $E_2$ . Since the transmissivity of the ball is zero [22]

$$\rho_b + \alpha_b = 1 \quad (9)$$

but at equilibrium [22]

$$\alpha_b = \epsilon_b \quad (10)$$

therefore

$$\rho_b = 1 - \epsilon_b \quad (11)$$

Equation (4) may now be rewritten for the experiments rising balls with low and high emissivity

$$E_1/k = 0.830(N_f + N_{b1}) + 1.598 N_s - .426 N_o \quad (12)$$

$$E_2/k = 0.830(N_f + N_{b2}) + 1.440 N_s - .556 N_o \quad (13)$$

where the subscript 1 refers to the low emissivity ( $\epsilon_{b1} = .28, \rho_{b1} = .72$ ) and 2 refers to the high emissivity ball ( $\epsilon_{b2} = .47, \rho_{b2} = .53$ ). Subtracting equation (12) from (13)

$$\frac{E_2 - E_1}{k} = 0.830 (N_{b2} - N_{b1}) - 0.158 N_s - .130 N_o \quad (14)$$

The black body radiance  $N^{BB}$  is a function of temperature only with

$$N = \epsilon N^{BB} \quad (15)$$

Since the ball surface temperatures are assumed equal in cases 1 and 2, equation (14) may be rewritten as

$$\frac{E_2 - E_1}{k} = 0.158 N_b^{BB} - .158 N_s - .130 N_o \quad (16)$$

With an ambient temperature of 25°C,  $N_o = 3.7 \times 10^{-3}$  watts/cm<sup>2</sup> - ster. A conservative estimate of  $N_s$  (see Appendix B) is on the order of  $0.4 \times 10^{-3}$  watts/cm<sup>2</sup> - ster or about 2 percent of  $N_b^{BB}$  and has, therefore, been neglected. The value of  $N_b^{BB}$  is typically of the order  $20 \times 10^{-3}$  watt/cm<sup>2</sup> - ster. The only unknown in equation (16) is  $N_b^{BB}$ . The temperature can be obtained from the black body radiance through the calibration curve supplied with radiometric detector.

Although the two experiments described above allow the determination of the ball surface temperature they are not sufficient to allow the film temperature to be deduced. The technique devised to isolate the film radiance consists of an experiment in which the low emissivity ball

is used. The detector output signal  $E_1$  is then compared with the signal  $E_3$  obtained with a filter placed between the upper sapphire surface and the detector objective (see Figure 8). The filter consists of a sandwich of two sapphire disks and a  $5 \times 10^{-5}$  m (0.002 in.) thick film of oil identical in composition to that being used in the EHD contact. Hence the radiation from the EHD oil film is absorbed by the oil in the filter. As can be seen from Figure 8, those contributions other than  $\eta_f N_f$  shown in Figure 7 have been attenuated by a filter attenuation factor  $\eta_F$ . Because of a strong absorption band (C-H bond) in the aliphatic oil at  $3.4\mu$ , the EHD oil film will emit primarily at this wave length. Since a much thicker film of the same oil is used in the filter, the filter will absorb the entire contribution  $\eta_f N_f$  from the EHD oil film. A reflecting shield is placed between the upper surface of the EHD contact sapphire and the filter until just prior to recording the total radiance to maintain the filter at ambient temperature. Otherwise, the absorption of  $\eta_f N_f$  would raise the filter temperature to some unknown value. Figure 8 also shows that the filter itself is emitting at  $T_0$  and that some of the background radiation is also reflected from the filter. The total radiance received in this third experiment is, therefore,

$$\left( \begin{array}{c} N \\ \text{TOTAL} \end{array} \right)_3 = \eta_F (\eta_{b1} N_{b1} + \eta_s N_s + \eta_o N_o) + \epsilon_F N_o + \rho_F N_o \quad (17)$$

Substituting equations (1) and (17) into equation (2) we get,

$$E_3/k = \eta_F (.830N_{b1} + 1.598N_s + .574N_o) - (1 - \rho_F - \epsilon_F) N_o \quad (18)$$

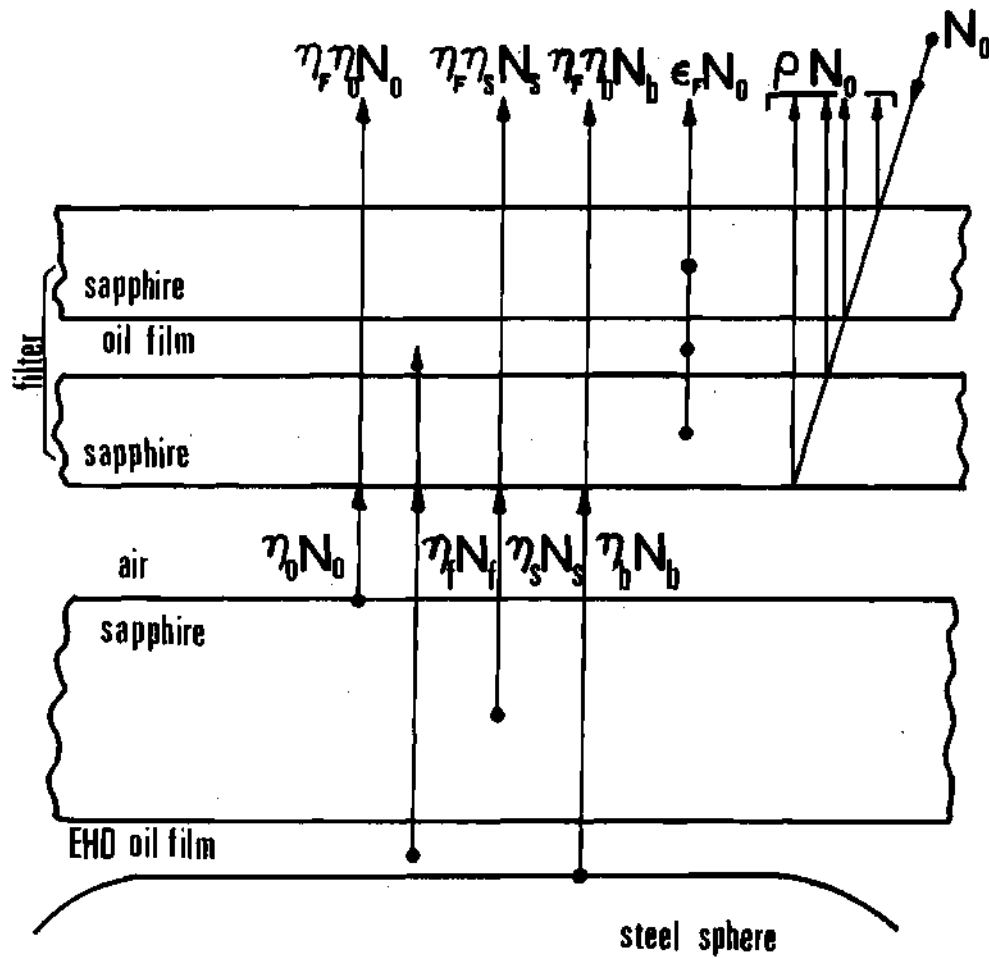


Figure 8. Oil Film Filter (Not to Scale).

Since for a transparent medium [22]

$$t_F + \rho_F + \epsilon_F = 1 \quad (19)$$

the last term in equation (18) may be written as  $t_F N_O$ . The transmissivity of the filter  $t_F$  can be related to the attenuation factor  $\eta_F$  which includes transmission and reflection losses

$$\eta_F = (1 - \rho_F) t_F = 0.850 t_F \quad (20)$$

where the reflection losses are calculated Fresnel reflections at the sapphire-air and sapphire-oil interfaces. Substitution of equation (20) into (18) and subtracting from equation (12) yields,

$$\left( E_1 - \frac{E_3}{\eta_F} \right) \frac{1}{k} = 0.830 N_f + 0.176 N_O = 0.830 \epsilon_f N_f^{BB} + 0.176 N_O \quad (21)$$

The quantities  $E_1$  and  $E_3$  are the output signals, and  $k$  and  $N_O$  are known. The film emissivity  $\epsilon_f$  can be obtained from equation (6) since the film thickness profile has also been obtained throughout the contact [23]. The filter attenuation factor has been found experimentally by placing the filter between the detector objective and a calibrated black body source (Barnes, Model RM 121). Because of the spectral shift in peak power wavelength with increasing temperature, this attenuation factor is a function of the equivalent black body source temperature. Using the black body source, a calibration curve of  $\eta_F$  as a function of temperature was obtained.

Based on an initial estimate of the EHD film temperature  $T_f$ , a value of  $\eta_f$  is inserted in equation (21) which is then solved for  $N_f^{BB}$ . The film temperature is then determined directly from this value. A better estimate of  $\eta_f$  can be used in equation (21) until convergence on a film temperature is obtained. Because the variation of  $\eta_f$  in the range of interest is small, convergence is rapid.

The procedure needed to obtain a mean film temperature and ball surface temperature, therefore, requires that four separate experiments be performed: the film thickness using optical interference methods and radiance data for the low emissivity ball with and without the oil film filter and the high emissivity ball without the filter. The success of the procedure is based on the fact that the data in the EHD experiment are reproducible (23) thereby assuring identical conditions in each of the four experiments.

In order to collect a large amount of data in a short period of time so that the contact temperatures will not change significantly, a scanning system has been built into the detector mount which permits the detector to scan through the contact area in the direction of the surface velocity. Data were taken continuously in the direction of the scan at a constant detector speed of 0.0075 in/sec. The infrared detector has a temperature resolution of 5°C corresponding to 0.01 sec response time. The temperature resolution improves to 0.5° C for a response time of 1.0 sec. Successive passes were made at  $2.5 \times 10^{-5}$  m (0.001 in) increments. From these data points, the contour maps shown in Figures 9 and 10 were

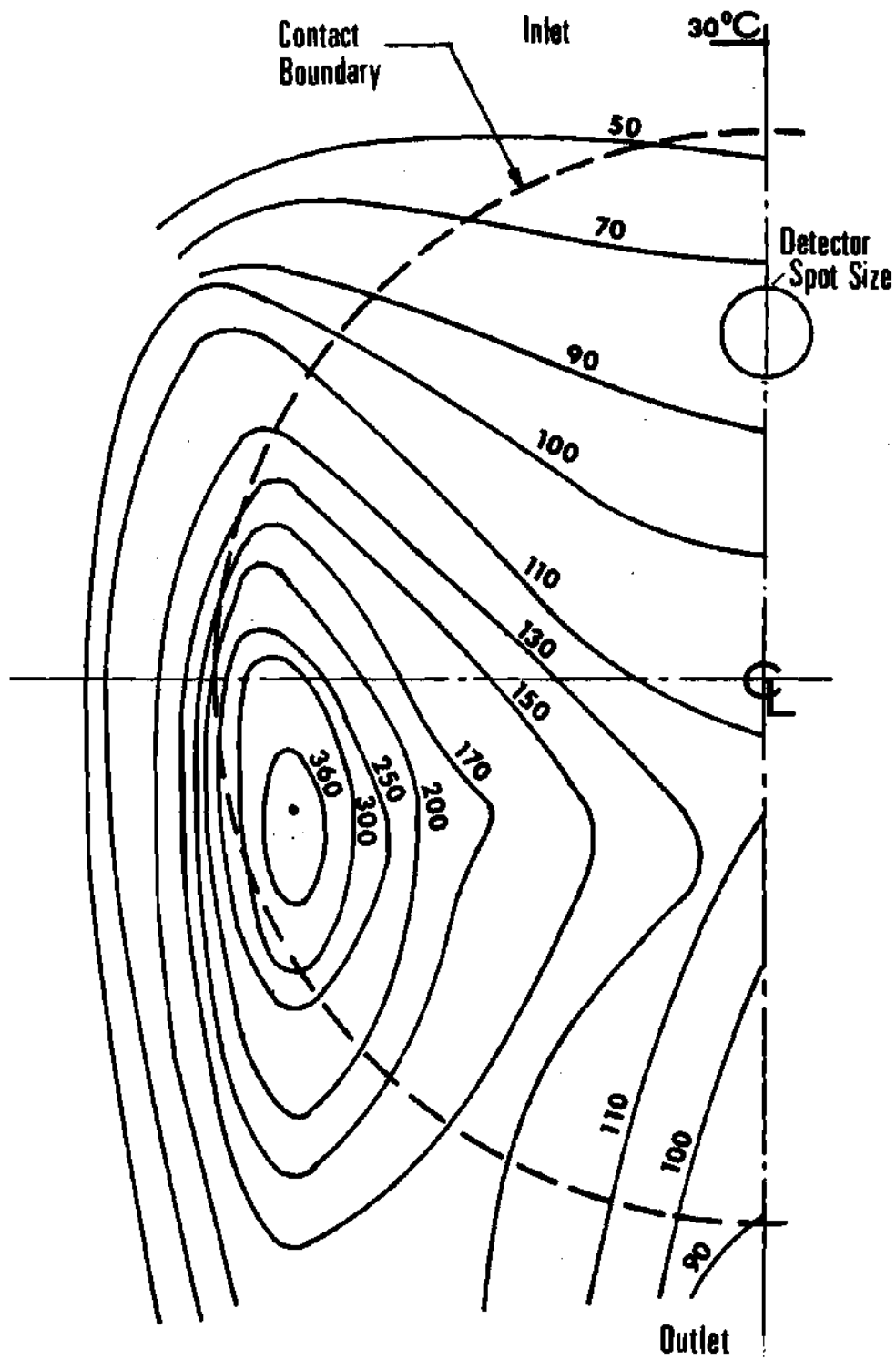


Figure 9. Steady State Film Temperature in the EHD Contact at 1.39 m/sec (54.9 ips) Sliding Speed.

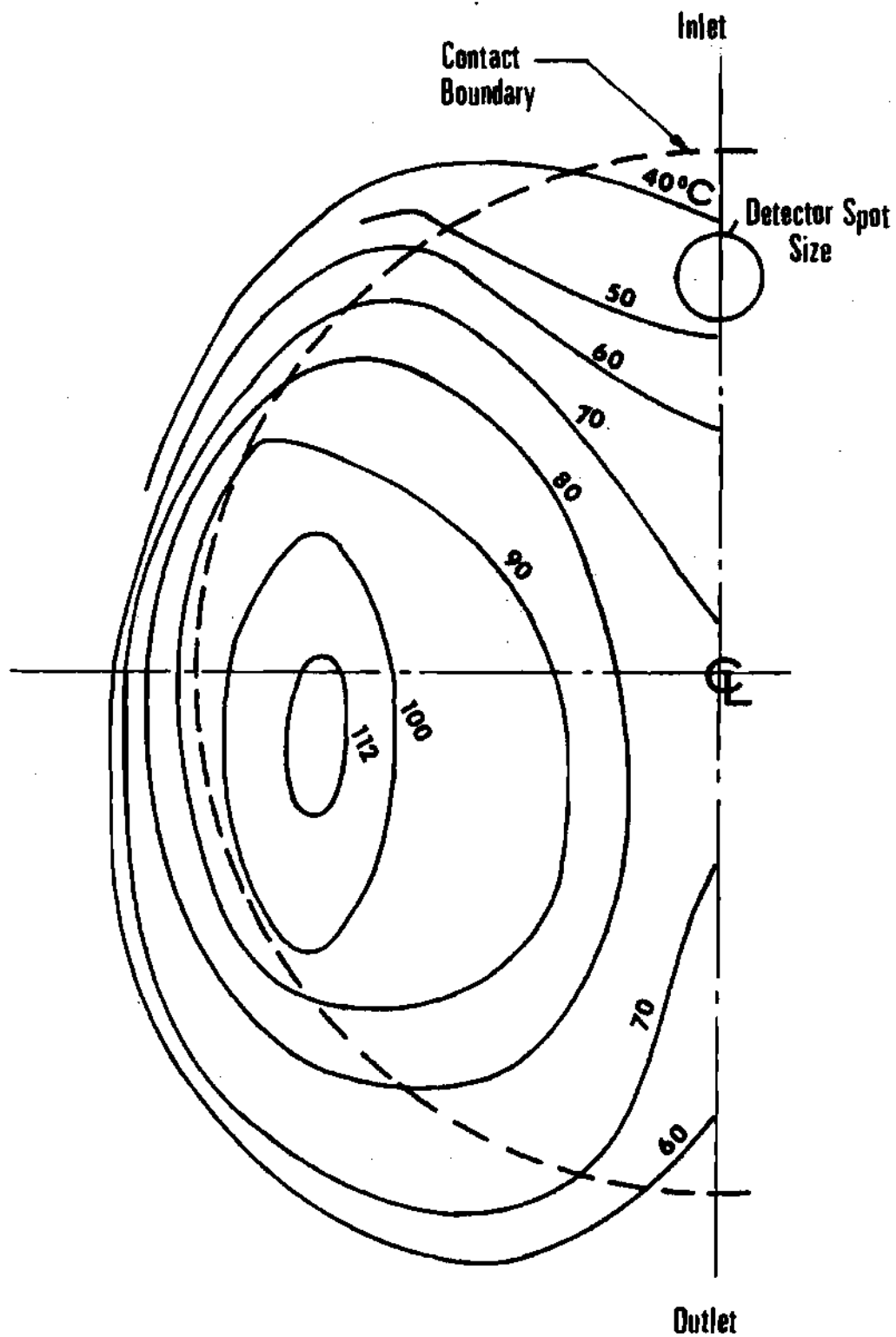


Figure 10. Ball Surface Temperature in the EHD Contact  
at 1.39 m/sec (54.9 ips) Sliding Speed.

developed. The recorded output  $E/k$  of the detector (see Tables 1 thru 3) serves directly as a map of total radiance as a function of contact position.

### Experimental Results

The lubricant used during this investigation is an aliphatic mineral oil used in previous EHD studies (11, 12, 23) and vis-cometric studies (24) in this laboratory. The fluid has been shown to be Newtonian (24) at shear rate and pressure levels approaching those anticipated in the EHD contact. The atmospheric pressure viscosity is  $0.0217 \text{ Ns/m}^2$  (21.7 cp) at 37.8 C and  $0.0032 \text{ Ns/m}^2$  (3.2 cp) at 98.9 C and the pressure-viscosity characteristic  $\alpha^*$  is  $2.32 \times 10^{-8} \text{ m}^2/\text{N}$  ( $1.60 \times 10^{-4} \text{ in}^2/\text{lbf}$ ).

All data was obtained with a peak Hertz contact pressure of  $1.034 \times 10^9 \text{ N/m}^2$  (150,000 psi). Sliding velocities of 0.35, 0.69 and 1.39m/s (13.7, 27.4 and 54.9 in/sec) were used in the investigation.

Using the optical techniques developed in the previous section, contour maps of the steady state film and ball surface temperatures have been obtained and are shown in Figures 9 and 10 for the maximum sliding velocity. In each of these figures the boundary of the Hertzian contact region is shown for reference. Since the EHD contact is assumed to be symmetric about the centerline only one half of the contact area has been studied. Figure 11 shows the interference fringe pattern for the same conditions

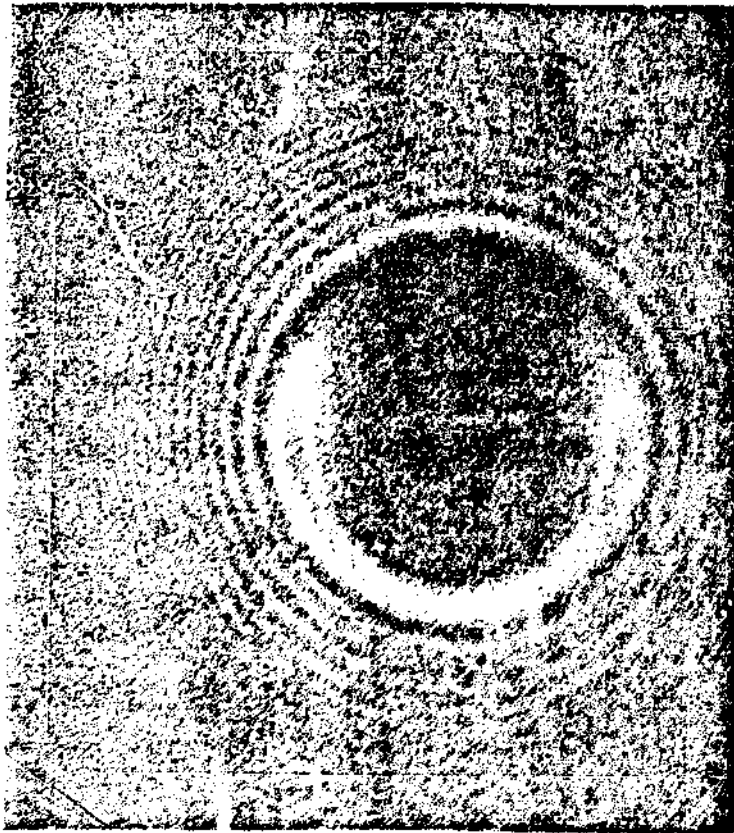


Figure 11. Interference Fringe Pattern of the EHD Contact  
at 1.39 m/sec (54.9 ips) Sliding Speed.

(1.39 m/s,  $1,034 \times 10^9$  N/m<sup>2</sup>) as used in Figures 9 and 10.

In all these figures, the lubricant is entering the contact at the top of the figure. Referring to Figure 9, it can be seen that along the contact centerline, the lubricant is at 30 C just ahead of the contact inlet and increases in temperature to almost 50 C as it crosses the Hertzian contact boundary. The film reaches a maximum of 115 C just beyond the contact center and exits from the contact region at 75 C. The most striking feature about Figure 9, however, is the fact that the maximum film temperature ( $\approx 360$  C) occurs at the minimum film thickness location (see Figure 11) in the EHD side lobe constriction. Based on previous measurements (23) the film thickness at this location is only  $6.35 \times 10^{-8}$  m ( $2.5 \times 10^{-6}$  in.).

Figure 10 is a plot of the ball surface temperature distribution. The ball surface temperature is less than 40 C at the contact inlet, rises to over 70 C just beyond the contact center and exits the contact at just under 60 C. As is the case for  $T_f$ , the maximum ball surface temperature occurs in the side lobe constriction. The maximum values of  $T_f$  and  $T_b$  do not appear to be at precisely the same locations, however. The maximum ball temperature is only 115 C compared with 360 C for the lubricant film.

The temperature contours shown in Figures 9 and 10 were the maximum steady state values obtained during the investigation. Figures 12, 13 show the variation with sliding velocity of steady temperature,  $T_f$  and  $T_b$  along the contact centerline. At each

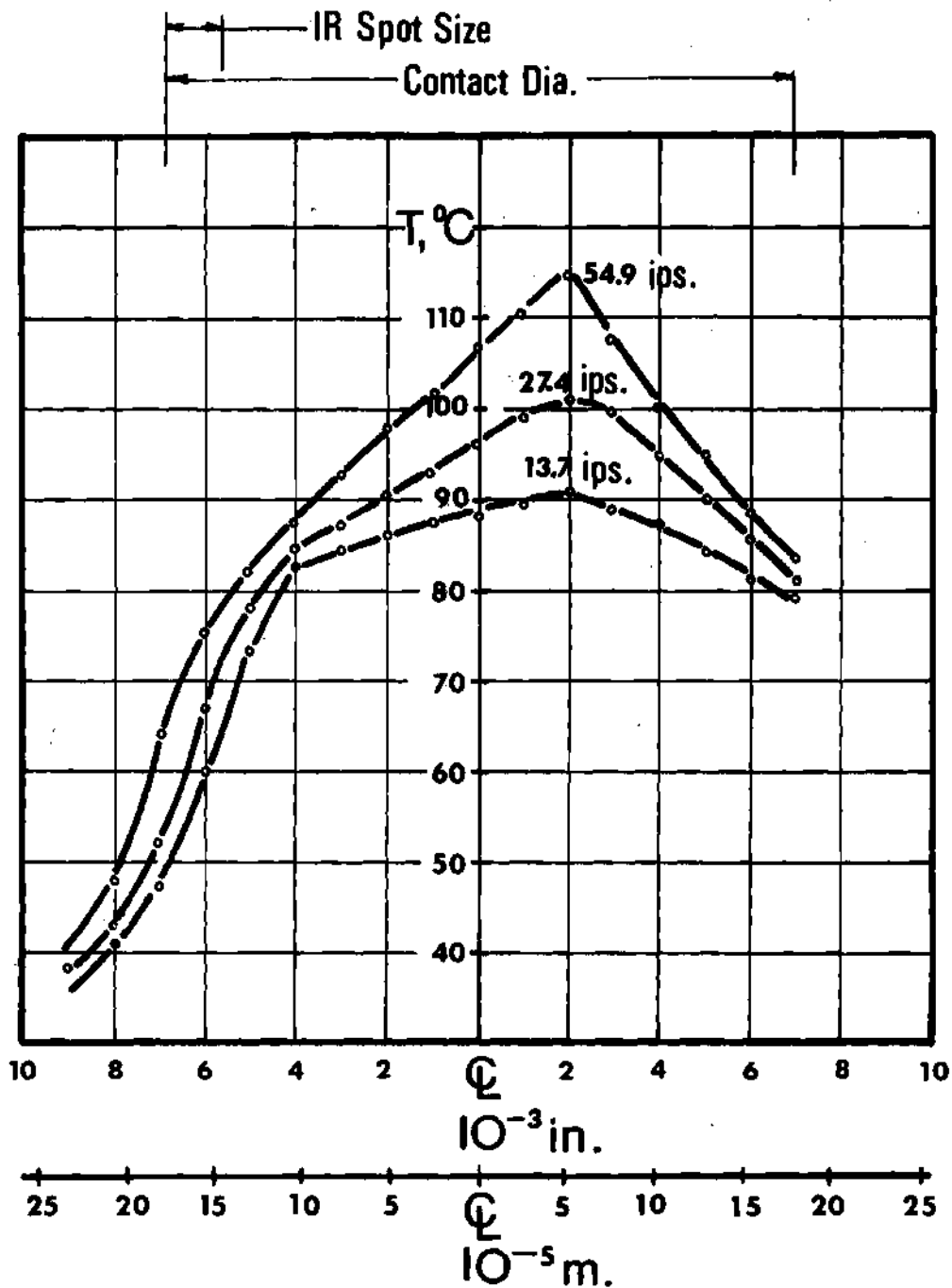


Figure 12. Steady State Film Temperature Distribution along the Contact Centerline as a Function of Sliding Speed.

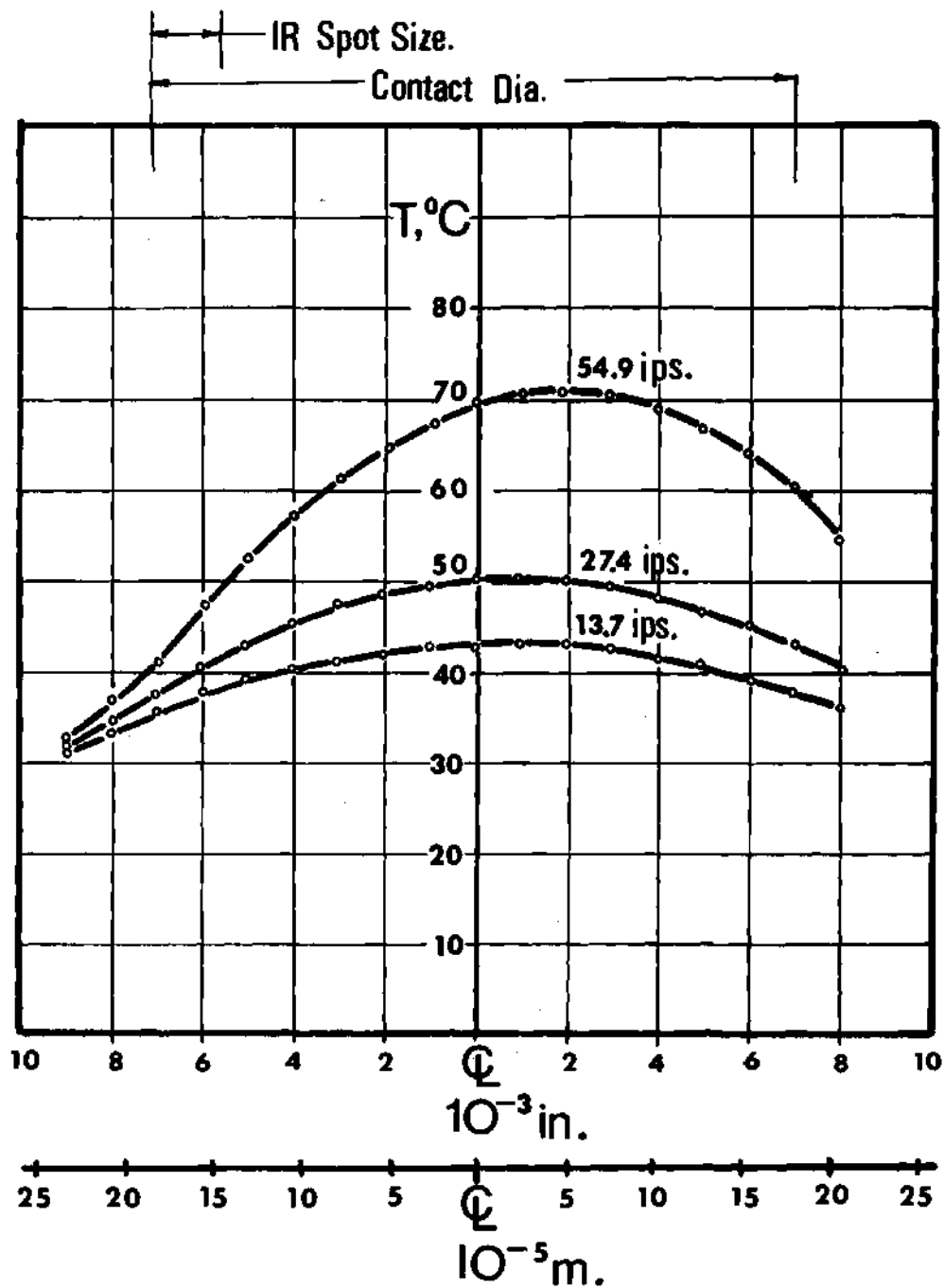


Figure 13. Ball Surface Temperature along the Contact Centerline as a Function of Sliding Speed.

position in the contact and at each speed, the mean film temperature is substantially higher than the ball surface temperature. This is consistent with the fact that there is internal heat generation in the film due to viscous shear and that conduction to the boundaries is a primary heat transfer mechanism.

Finally, Figure 14 is a plot of maximum ball surface temperature in the contact as a function of sliding velocity. As was mentioned above, the maximum temperature is found in the EHD side lobe constriction. Figure 14 also shows the film temperature variation with sliding velocity at the same contact location where the maximum ball temperature was found. Due to significant film emissivity variation throughout the contact, this location, which is the point of maximum radiance, is not necessarily the point of maximum  $T_f$ . Except for the highest sliding velocity experiment, sufficient data were not obtained to find the maximum fluid temperature in the side lobe constriction.

#### Discussion of Results

The most useful temperature data which could be obtained for an EHD contact would be the sapphire and ball surface temperatures plus the temperature profile through the lubricant film. We have presented a technique wherein the actual ball surface temperature and a fourth power average fluid temperature taken through the film can be determined. The fact that the fourth power average is determined means that the peak film temperatures will be somewhat

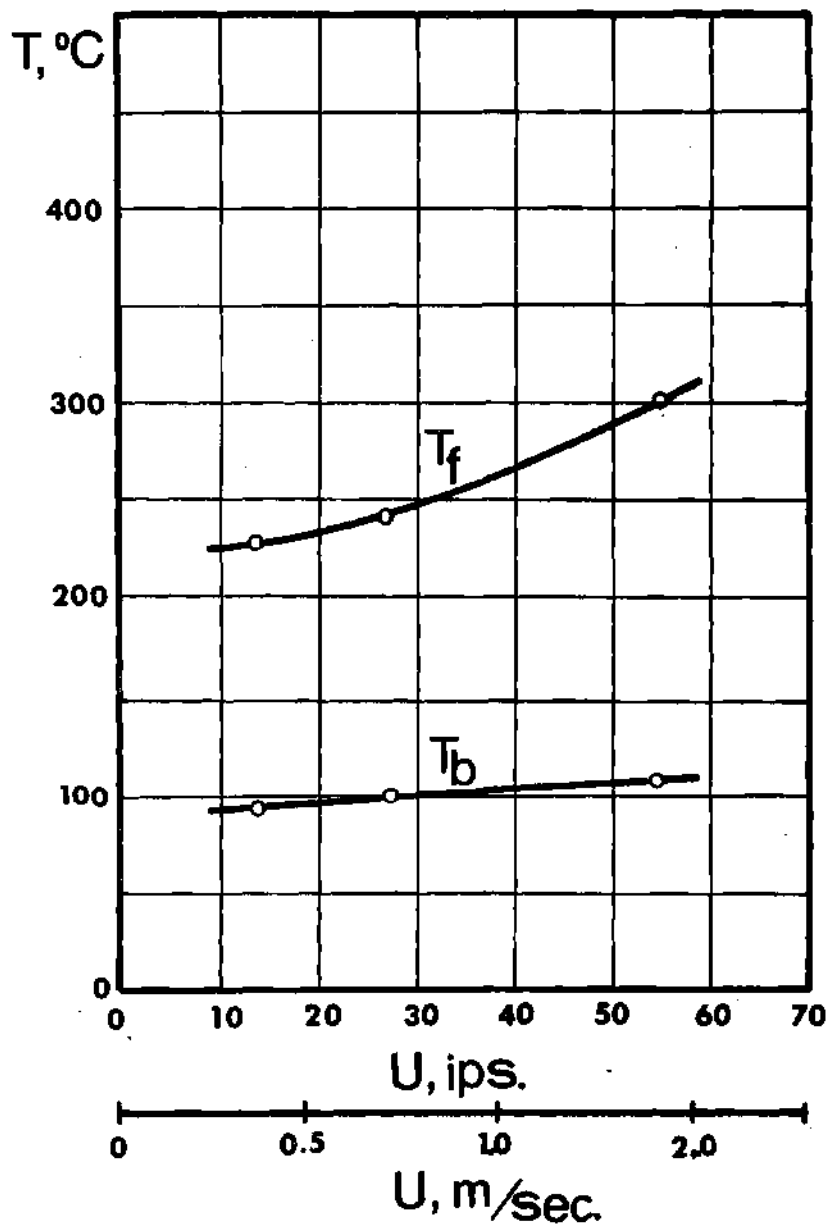


Figure 14. Maximum Ball Surface Temperature and Film Temperature as a Function of Sliding Speed.

will be somewhat higher than the data presented.

Throughout the above discussion film thickness data has been used which was taken in a separate experiment with essentially the same apparatus. In the film thickness investigations, a  $3.18 \times 10^{-3}$  m (.125 in) thick sapphire was used whereas a  $1.52 \times 10^{-3}$  m (.060 in) sapphire was used in IR investigations. Because the thickness of the sapphire may influence its temperature distribution, thus changing the thermal boundary condition in the contact, film thickness and traction data were taken using both sapphires and were found to be identical.

The detector has been calibrated over the temperature range of interest using a radiometric calibration source (Barnes Model RM-121). The detector resolution under the conditions of the experiment is 0.5C according to manufacturer's specifications. Because of this relatively high resolution, the accuracy of the temperature data reported is primarily a function of the emissivity values and the proportion of received radiance assigned to each source in equations (15, 16, 21). The measured emissivity values for the ball surface used are believed to be correct to well within 10 %. If this  $\pm 10\%$  error is carried through the above equations it amounts to an error in ball temperature of  $\pm 4^{\circ}\text{C}$  at the maximum contact temperature of 115 C. At locations where the temperature is less than this maximum the error will be lower. Also, if any of the calculated coefficients in equations (16) and (21) are in error by  $\pm 10\%$ , a similar error in ball temperature

will result.

The most significant possible error is in the emissivity assigned to the oil film. From equation (6) it is seen that the emissivity is proportional to film thickness. Unfortunately, the error in film thickness is an absolute quantity (depending on fringe order interpretation (see Figure 11) rather than a percentage of the film thickness. This yields a maximum relative error at points of minimum film thickness, which are located at the points of maximum film temperature. The maximum error in film thickness has been assessed at  $\pm 1.8 \times 10^{-8} \text{ m}$  ( $0.7 \times 10^{-6} \text{ in}$ ) corresponding to misreading a contour on the film fringe pattern. At the point of maximum film temperature (360 C) this  $\pm 1.8 \times 10^{-8} \text{ m}$  error in minimum film thickness ( $6.4 \times 10^{-8} \text{ m}$ ) results in an error in temperature of  $\pm 30^\circ \text{ C}$ . At all other locations within the contact, this error is substantially less because the film thickness is larger and the error in reading represents in this case only a fraction of its actual value. Also, for investigations in which the minimum film thickness is greater than  $6.4 \times 10^{-8} \text{ m}$ , which includes most cases previously investigated in this laboratory (11, 12, 23), the magnitude of the error is expected to be lower.

The extremely high local fluid temperatures found in this investigation are thought to be a result of the high shear rates ( $10^7 \text{ sec}^{-1}$ ) at minimum film thickness locations in the Hertzian contact. The question does arise, however, whether the shearing is viscous with complete separation of the surfaces, or there is

actually some asperity contact at the minimum film thickness locations. This is a possibility for the cases reported above since the minimum film thicknesses in the side lobes are of the order of the surface roughness values for the ball and sapphire. It is not obvious if asperity contact is occurring, however, since the ball surface shows no surface damage after running under load for several minutes. An investigation is currently under way (25) to determine which mechanism is causing these extreme temperature values.

In this research (25) a model was developed to determine the relationship between the adiabatic stationary wall temperature  $T_{mw}$ , which is the maximum fluid temperature and the moving wall temperature,  $T_1$ . This model is based on the assumptions that the only heat source is the viscous dissipation and at constant shear stress rate. It results in a relationship of the form,

$$\int_{T_1}^{T_{mw}} \frac{K_T}{n(p,T)} dT = U^2 \quad (22)$$

where:

- $K_T$  = thermal conductivity  
= 0.0167 lbf/sec ° F
- $n(p,T)$  = fluid viscosity function of the local pressure  
and temperature
- $U$  = sliding speed

It should be noticed that the average fluid temperature, mapped in the Figure 9, has to be at any time smaller than that of the adiabatic stationary wall temperature, unless some additional heat sources other than viscous dissipation in the fluid are present. The equation (22) was solved graphically for the maximum wall temperature due to viscous dissipation. This temperature obtained from the analysis was found to exceed in some regions the lubricant temperature experimentally deduced. The findings indicate the existence of a region in the contact area where a heat source, other than viscous dissipations, influences the lubricant temperature (Figure 15). In the conditions under investigation the asperity contact is assumed to be the additional energy source causing the high fluid temperature.

As seen in Figure 15, part of the area where the asperity contact may be present corresponds to that expected as a result of small film thicknesses in the side lobes. The roughness of the sphere used is  $3.18 \times 10^{-8} \text{ m}$  ( $1.3 \times 10^{-6} \text{ in}$ ) and the minimum film thickness for a speed of 1.39 m/sec (54.9 in/sec) and load of 6.8 Kgf (15 lbf) is  $6.35 \times 10^{-8} \text{ m}$  ( $2.5 \times 10^{-6} \text{ in}$ ).

If the asperity contact plays an important role in causing the high fluid temperature, the infrared technique can be an useful tool in detecting incipient film failure in highly loaded contacts.

#### Conclusions

The author has presented a technique for mapping the temperature distribution in a sliding EHD contact. Both the ball surface

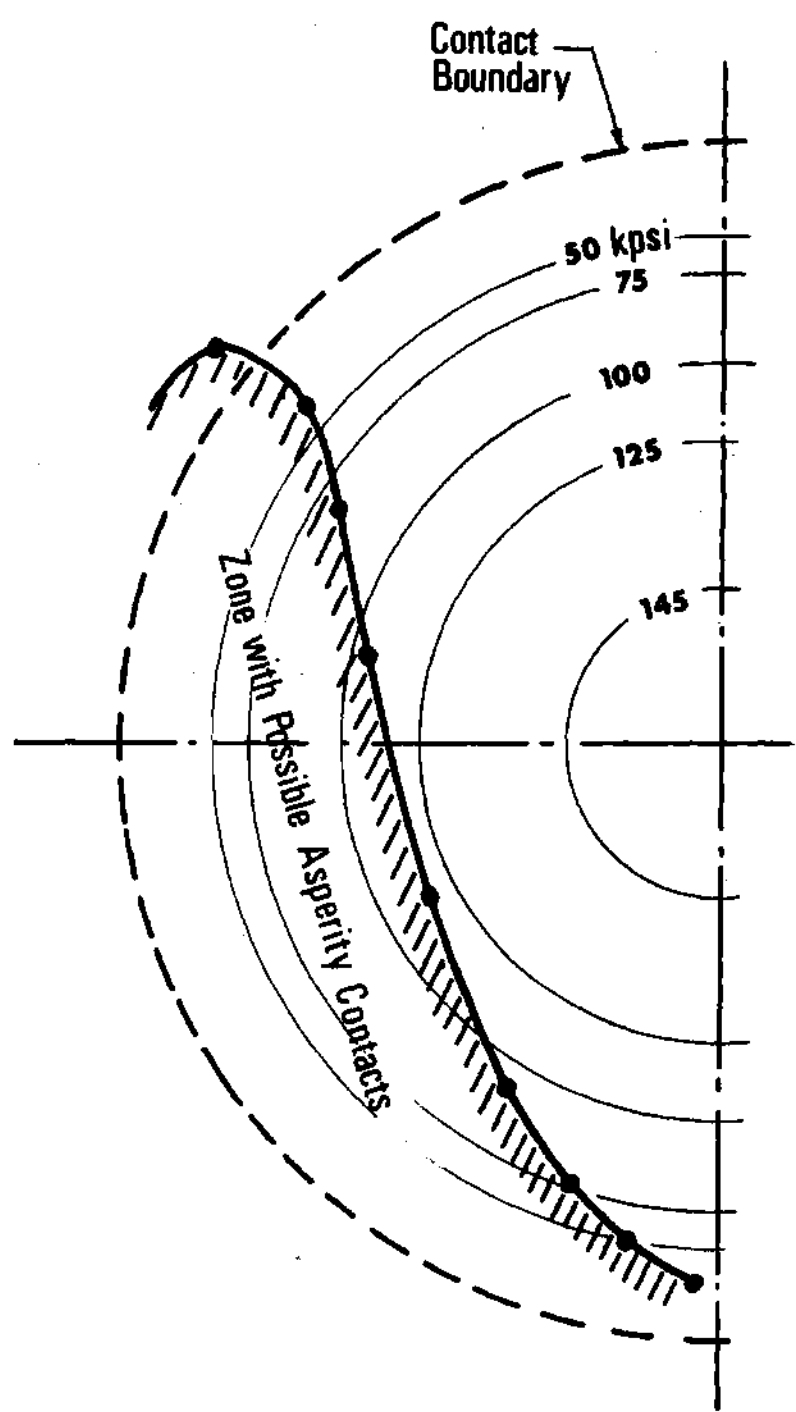


Figure 15. Contact Region with External Heat Source (Asperity Contacts).

temperature and a fourth power average lubricant film temperature have been obtained at points throughout the contact. Under a specific set of experimental conditions, ball temperatures as high as 115 C and average fluid film temperatures as high as 360 C have been reported. Both temperature peaks were found to occur in the contact side lobes where the film thickness is a minimum. It was also observed that at each point in the contact, both temperatures increased significantly as the sliding velocity was increased.

Although only a limited amount of data was collected, it is sufficient to show that the technique reported can be useful in obtaining detailed temperature data in the EHD contact. In addition, it also suggests additional experiments using the IR microdetector; namely extensions to rolling contact experiments, to a determination of the sapphire surface temperature, to a spectral analysis of the materials in the contact, to aid in evaluating lubricant constitutive equations under EHD conditions, and to an investigation of the mechanisms leading to film failure.

Table 1. Experimental Data for Speed of 1.39 m/sec  
(54.9 ips) and Load of 6.8 Kgf (15 lbf).

Location	$E_1/k$	$E_2/k$	$E_3/k$	$\eta_F$	$\epsilon_f$	$T_B$	$T_f$
x,y	$\frac{\text{mW}}{\text{cm}^2\text{-ster}}$	$\frac{\text{mW}}{\text{cm}^2\text{-ster}}$	$\frac{\text{mW}}{\text{cm}^2\text{-ster}}$	%	$\times 10^3$	$^{\circ}\text{C}$	$^{\circ}\text{C}$
0,8	1.51	1.91	0.35	41.0	1.80	37	47
0,7	1.57	2.05	0.37	41.0	1.68	41	65
0,6	1.64	2.35	0.40	42.0	1.44	47	70
0,5	1.73	2.60	0.40	42.5	1.44	52	76
0,4	1.84	2.92	0.50	43.0	1.44	57	85
0,3	1.99	3.25	0.58	44.0	1.44	61	92
0,2	2.24	3.70	0.70	45.0	1.44	65	98
0,1	2.51	4.10	0.85	46.5	1.44	67	101
0,0	2.82	4.50	1.00	47.0	1.44	68	107
0,-1	2.93	4.75	1.07	48.0	1.44	70	110
0,-2	3.03	4.86	1.13	48.5	1.44	71	115
0,-3	2.96	4.78	1.10	48.5	1.44	70	106
0,-4	2.87	4.60	1.05	48.0	1.44	69	92
0,-5	2.78	4.40	1.00	47.5	1.56	67	84
0,-6	2.64	4.10	0.92	46.5	1.20	65	80
0,-7	2.54	3.75	0.86	46.0	1.80	60	82
0,-8	-	-	-	-	-	-	-

Table 1. (cont'd).

Location	$E_1/k$	$E_2/k$	$E_3/k$	$\eta_F$	$\epsilon_f$	$T_B$	$T_f$
x,y	$\frac{\text{mW}}{\text{cm}^2\text{-ster}}$	$\frac{\text{mW}}{\text{cm}^2\text{-ster}}$	$\frac{\text{mW}}{\text{cm}^2\text{-ster}}$	%	$\times 10^3$	$^{\circ}\text{C}$	$^{\circ}\text{C}$
1,8	1.75	2.15	0.42	39.0	2.40	37	48
1,7	1.87	2.35	0.47	39.0	1.68	41	66
1,6	2.03	2.60	0.53	39.0	1.53	44	73
1,5	2.20	3.10	0.60	39.5	1.53	53	80
1,4	2.43	3.65	0.70	40.0	1.53	60	87
1,3	2.68	4.25	0.80	40.0	1.53	66	95
1,2	2.94	5.00	0.90	40.0	1.53	75	100
1,1	3.37	5.65	1.07	40.0	1.53	77	107
1,0	3.81	6.10	1.26	40.5	1.53	77	110
1,-1	4.14	6.45	1.41	41.0	1.53	78	115
1,-2	4.31	6.63	1.49	41.5	1.53	78	130
1,-3	4.14	6.43	1.40	41.0	1.53	77	130
1,-4	3.87	6.10	1.30	41.0	1.53	76	115
1,-5	3.73	5.80	1.22	40.5	2.16	75	105
1,-6	3.60	5.35	1.17	40.0	1.20	72	95
1,-7	3.42	4.75	1.10	40.0	0.96	63	90
1,-8	-	-	-	-	-	-	-

Table 1. (cont'd).

Location	$E_1/k$	$E_2/k$	$E_3/k$	$\eta_F$	$\epsilon_f$	$T_B$	$T_f$
x,y	$\frac{\text{mW}}{\text{cm}^2\text{-ster}}$	$\frac{\text{mW}}{\text{cm}^2\text{-ster}}$	$\frac{\text{mW}}{\text{cm}^2\text{-ster}}$	%	$\times 10^3$	$^{\circ}\text{C}$	$^{\circ}\text{C}$
2,8	1.87	2.25	0.47	39.0	2.40	37	50
2,7	1.95	2.61	0.50	39.0	1.68	46	66
2,6	2.21	3.05	0.60	39.0	1.53	52	75
2,5	2.57	3.70	0.74	39.0	1.53	58	83
2,4	2.93	4.50	0.90	40.0	1.53	66	90
2,3	3.49	5.50	1.12	40.0	1.53	74	98
2,2	4.06	6.40	1.35	40.0	1.53	78	104
2,1	4.70	7.13	1.60	41.0	1.53	80	108
2,0	5.03	7.80	1.82	42.0	1.53	84	110
2,-1	5.37	8.20	2.00	43.0	1.53	85	130
2,-2	5.45	8.43	2.05	43.5	1.53	86	143
2,-3	5.40	8.28	2.03	43.5	1.53	85	140
2,-4	5.37	8.00	2.00	43.0	1.68	83	130
2,-5	5.16	7.63	1.90	43.0	2.16	81	125
2,-6	4.88	6.85	1.76	42.0	0.96	74	120
2,-7	4.50	6.07	1.60	42.0	1.20	66	115
2,-8	4.07	5.50	1.35	40.0	2.40	64	110

Table 1. (cont'd).

Location	$E_1/k$	$E_2/k$	$E_3/k$	$\eta_F$	$\epsilon_F$	$T_B$	$T_f$
x,y	$\frac{\text{mW}}{\text{cm}^2\text{-ster}}$	$\frac{\text{mW}}{\text{cm}^2\text{-ster}}$	$\frac{\text{mW}}{\text{cm}^2\text{-ster}}$	%	$\times 10^3$	$^{\circ}\text{C}$	$^{\circ}\text{C}$
3,8	2.20	2.60	0.60	39.0	2.88	37	50
3,7	2.60	3.05	0.75	39.0	2.40	40	67
3,6	3.03	3.90	0.92	39.0	1.68	52	78
3,5	3.59	5.00	1.15	39.5	1.53	62	85
3,4	4.14	6.25	1.40	40.5	1.53	76	95
3,3	4.61	7.30	1.61	41.0	1.53	85	100
3,2	5.10	8.25	1.85	42.0	1.53	88	107
3,1	5.58	9.00	2.10	43.0	1.53	93	116
3,0	6.08	9.60	2.36	44.0	1.53	94	130
3,-1	6.63	10.20	2.65	45.0	1.53	95	145
3,-2	6.85	10.50	2.80	46.0	1.53	95	155
3,-3	6.63	10.20	2.70	46.0	1.53	95	150
3,-4	6.44	9.90	2.55	45.0	1.92	93	147
3,-5	6.08	9.15	2.35	44.0	1.44	87	145
3,-6	5.87	8.45	4.25	43.5	0.96	80	140
3,-7	5.86	7.50	2.20	43.0	1.68	67	137
3,-8	5.84	7.10	2.18	43.0	2.63	60	132

Table 1. (cont'd).

Location	$E_1/k$	$E_2/k$	$E_3/k$	$\eta_F$	$\epsilon_f$	$T_B$	$T_f$
x,y	$\frac{\text{mW}}{\text{cm}^2\text{-ster}}$	$\frac{\text{mW}}{\text{cm}^2\text{-ster}}$	$\frac{\text{mW}}{\text{cm}^2\text{-ster}}$	%	$\times 10^3$	$^{\circ}\text{C}$	$^{\circ}\text{C}$
4,8	2.52	3.00	0.72	39.0	3.36	42	50
4,7	2.98	3.75	0.90	39.0	2.40	49	68
4,6	3.42	4.90	1.10	40.0	1.53	65	80
4,5	3.98	6.05	1.32	40.0	1.53	75	90
4,4	4.51	7.20	1.57	41.0	1.53	83	97
4,3	4.98	8.20	1.80	42.0	1.53	88	105
4,2	5.40	9.10	2.02	43.0	1.53	93	115
4,1	5.90	9.70	2.28	44.0	1.53	96	130
4,0	6.29	10.35	2.50	45.0	1.53	97	140
4,-1	6.86	10.90	2.80	46.0	1.53	97	160
4,-2	6.97	11.00	2.90	47.0	1.53	98	170
4,-3	6.87	10.70	2.80	46.0	1.53	97	165
4,-4	6.66	10.15	2.70	46.0	1.80	94	160
4,-5	6.38	9.40	2.55	45.0	0.96	88	155
4,-6	6.05	8.75	2.38	44.5	0.72	82	150
4,-7	5.80	8.10	2.20	44.0	2.40	77	145
4,-8	5.64	7.50	2.10	43.5	3.36	70	135

Table 1. (cont'd).

Location	$E_1/k$	$E_2/k$	$E_3/k$	$\eta_F$	$\epsilon_f$	$T_B$	$T_f$
x,y	$\frac{\text{mW}}{\text{cm}^2\text{-ster}}$	$\frac{\text{mW}}{\text{cm}^2\text{-ster}}$	$\frac{\text{mW}}{\text{cm}^2\text{-ster}}$	%	$\times 10^3$	$^{\circ}\text{C}$	$^{\circ}\text{C}$
5,8	2.73	3.10	0.80	39.0	3.84	38	50
5,7	3.00	4.35	0.90	39.0	2.88	62	70
5,6	3.37	5.60	1.05	39.0	2.16	76	83
5,5	3.93	6.85	1.30	40.0	1.53	86	95
5,4	4.63	8.00	1.62	41.0	1.53	90	98
5,3	5.35	9.15	2.00	43.0	1.53	95	110
5,2	5.95	10.05	2.30	44.0	1.53	96	130
5,1	6.62	10.75	2.70	46.0	1.53	97	150
5,0	7.13	11.35	3.05	48.0	1.53	98	160
5,-1	7.61	11.85	3.40	50.0	1.53	99	175
5,-2	7.80	12.00	3.55	51.0	1.53	99	185
5,-3	7.68	11.85	3.50	51.0	1.53	98	180
5,-4	7.61	11.25	3.40	50.0	1.53	94	175
5,-5	7.37	10.60	3.25	49.0	0.96	90	170
5,-6	7.15	9.90	3.05	48.0	1.68	84	160
5,-7	6.78	9.10	2.75	46.0	2.40	78	150
5,-8	6.78	8.50	2.72	46.0	3.84	71	140

Table 1. (cont'd).

Location	$E_1/k$	$E_2/k$	$E_3/k$	$\eta_F$	$\epsilon_f$	$T_B$	$T_f$
x,y	$\frac{\text{mW}}{\text{cm}^2\text{-ster}}$	$\frac{\text{mW}}{\text{cm}^2\text{-ster}}$	$\frac{\text{mW}}{\text{cm}^2\text{-ster}}$	%	$\times 10^3$	$^{\circ}\text{C}$	$^{\circ}\text{C}$
6,7	2.90	3.30	0.90	41.0	3.84	38	70
6,6	3.35	4.70	1.10	41.5	2.88	62	85
5,5	4.00	6.00	1.42	43.0	2.16	73	100
6,4	4.56	7.25	1.72	44.5	1.44	83	115
6,3	5.14	8.70	2.05	46.0	0.72	94	135
6,2	5.74	9.90	2.42	48.0	0.72	98	150
6,1	6.17	11.20	2.70	49.5	0.72	104	170
6,0	6.82	12.30	3.10	51.0	0.72	110	190
6,-1	7.44	13.10	3.50	53.0	0.72	112	240
6,-2	8.06	13.40	3.80	54.0	0.72	108	300
6,-3	7.85	13.10	3.73	54.0	0.72	107	280
6,-4	7.73	12.80	3.60	53.0	0.96	106	250
6,-5	7.32	12.10	3.40	53.0	1.44	104	210
6,-6	7.00	11.20	3.10	51.0	2.40	95	180
6,-7	-	-	-	-	-	-	-
6,-8	-	-	-	-	-	-	-

Table 1. (cont'd).

Location	$E_1/k$	$E_2/k$	$E_3/k$	$\eta_F$	$\epsilon_f$	$T_B$	$T_f$
x,y	$\frac{\text{mW}}{\text{cm}^2\text{-ster}}$	$\frac{\text{mW}}{\text{cm}^2\text{-ster}}$	$\frac{\text{mW}}{\text{cm}^2\text{-ster}}$	%	$\times 10^3$	$^{\circ}\text{C}$	$^{\circ}\text{C}$
7,7	2.20	2.60	0.60	40.0	3.84	38	73
7,6	2.63	3.85	0.83	40.7	3.36	61	90
7,5	3.15	5.30	1.00	41.5	2.88	75	107
7,4	3.96	6.60	1.40	43.0	2.40	81	120
7,3	4.70	8.00	1.80	45.0	0.72	90	150
7,2	5.52	9.40	2.25	47.0	0.72	95	177
7,1	6.35	11.00	2.73	49.5	0.72	102	222
7,0	7.25	12.30	3.20	52.0	0.72	107	305
7,-1	8.02	13.10	3.72	54.0	0.60	108	340
7,-2	8.33	13.38	3.90	55.0	0.60	107	370
7,-3	8.15	13.15	3.80	54.0	0.60	105	345
7,-4	7.90	12.60	3.65	53.5	0.72	103	312
7,-5	7.65	11.80	3.35	53.0	2.40	100	240
7,-6	7.25	11.00	3.10	52.0	2.88	96	215
7,-7	6.75	10.15	2.85	50.5	3.36	90	192
7,-8	6.30	9.30	2.60	49.0	3.84	86	165
7,-9	-	-	-	-	-	-	-

Table 1. (cont'd).

Location	$E_1/k$	$E_2/k$	$E_3/k$	$\eta_F$	$\epsilon_F$	$T_B$	$T_f$
x,y	$\frac{\text{mW}}{\text{cm}^2\text{-ster}}$	$\frac{\text{mW}}{\text{cm}^2\text{-ster}}$	$\frac{\text{mW}}{\text{cm}^2\text{-ster}}$	%	$\times 10^3$	$^{\circ}\text{C}$	$^{\circ}\text{C}$
8,8	-	-	-	-	-	-	-
8,7	-	-	-	-	-	-	-
8,6	-	-	-	-	-	-	-
8,5	4.02	5.00	1.30	40.0	3.84	53	105
8,4	4.66	6.00	1.60	41.0	3.20	62	115
8,3	5.40	7.00	2.00	43.0	2.88	67	120
8,2	6.12	8.00	2.35	44.0	2.04	73	150
8,1	6.78	9.00	2.70	46.0	1.67	77	200
8,0	7.40	9.80	3.10	49.0	1.44	80	250
8,-1	8.15	10.20	3.40	50.0	1.67	75	280
8,-2	8.80	10.70	3.60	51.0	2.04	72	270
8,-3	8.55	10.30	3.55	50.0	2.88	70	240
8,-4	7.95	9.50	3.40	50.0	3.20	68	200
8,-5	7.53	8.70	3.25	50.0	3.84	60	160
8,-6	-	-	-	-	-	-	-
8,-7	-	-	-	-	-	-	-
8,-8	-	-	-	-	-	-	-

Table 2. Experimental Data for Speed of 0.69 m/sec  
(27.4 in/sec) and Load of 6.8 Kgf (15 lbf).

Location	$E_1/k$	$E_2/k$	$E_3/k$	$\eta_F$	$\epsilon_f$	$T_B$	$T_f$
x,y	$\frac{\text{mW}}{\text{cm}^2\text{-ster}}$	$\frac{\text{mW}}{\text{cm}^2\text{-ster}}$	$\frac{\text{mW}}{\text{cm}^2\text{-ster}}$	%	$\times 10^3$	$^{\circ}\text{C}$	$^{\circ}\text{C}$
0,8	1.25	1.50	0.23	39.0	2.90	32	41
0,7	1.32	1.65	0.26	39.0	1.20	35	45
0,6	1.45	1.80	0.31	39.0	0.72	37	60
0,5	1.55	1.95	0.35	39.0	0.60	38	73
0,4	1.66	2.10	0.39	39.0	0.40	39	83
0,3	1.78	2.24	0.44	39.0	0.40	40	84
0,2	1.91	2.37	0.49	39.0	0.40	40	86
0,1	2.04	2.51	0.54	39.0	0.40	40	87
0,0	2.09	2.57	0.56	39.0	0.40	41	88
0,-1	2.15	2.65	0.585	39.5	0.40	42	89
0,-2	2.20	2.71	0.60	39.5	0.40	43	90
0,-3	2.16	2.66	0.585	39.5	0.40	42	89
0,-4	2.11	2.60	0.565	39.5	0.40	41	88
0,-5	2.03	2.50	0.535	39.5	0.50	40	84
0,-6	1.97	2.40	0.51	39.0	0.60	39	82
0,-7	1.89	2.25	0.475	39.0	0.35	37	79
6,-1	7.00	11.05	2.45	43.0	0.35	96	230

Table 3. Experimental Data for Speed of 0.35 m/sec  
(13.7 in/sec) and Load of 6.8 Kgf (15 lbf).

Location	$E_1/k$	$E_2/k$	$E_3/k$	$\eta_F$	$\epsilon_f$	$T_B$	$T_F$
x,y	$\frac{mW}{cm^2-ster}$	$\frac{mW}{cm^2-ster}$	$\frac{mW}{cm^2-ster}$	%	$\times 10^3$	$^{\circ}C$	$^{\circ}C$
0,8	1.44	1.73	0.30	39.0	3.60	34	42
0,7	1.59	2.03	0.35	39.0	2.15	37	52
0,6	1.69	2.70	0.40	39.0	1.20	40	60
0,5	1.80	3.14	0.45	39.0	0.96	43	73
0,4	1.94	2.32	0.50	39.0	0.96	45	80
0,3	2.07	2.50	0.55	39.0	0.96	47	87
0,2	2.23	2.68	0.61	39.0	0.96	48	90
0,1	2.36	2.86	0.66	39.0	0.96	49	93
0,0	2.48	3.00	0.715	39.0	0.96	50	96
0,-1	2.57	3.14	0.742	39.0	0.96	50	99
0,-2	2.61	3.20	0.755	39.0	0.96	50	101
0,-3	2.59	3.16	0.747	39.0	0.96	49	99
0,-4	2.51	3.05	0.718	39.0	0.96	48	87
0,-5	2.41	2.90	0.68	39.0	0.96	47	80
0,-6	2.30	2.73	0.64	39.0	0.96	45	79
0,-7	2.20	2.58	0.60	39.0	0.82	43	80
6,-1	7.05	11.30	2.38	43.0	0.82	100	240

## APPENDIX A

The Effect of Ball Radiation Change on Film Temperature

The energy dissipation rate in the EHD contact can be determined from film thickness and traction measurements previously obtained (11, 12). For the most severe conditions imposed in this investigation (1.39 m/s velocity and 67N normal load) the traction force was observed to be 4.7N. This results in an energy input rate (f.U) of 6.53 watts.

From radiance measurements made with each of the two balls, the change in ball radiation is of the order  $10^{-2}$  watts/cm<sup>2</sup> steradian for a  $3.6 \times 10^{-5}$ m diameter spot size. For radiation to one hemisphere ( $2\pi$  steradians) and for an EHD contact diameter of  $3.6 \times 10^{-4}$ m, the radiation heat transfer rate is of the order  $10^{-5}$  watts. Therefore, the heat transfer through the film due to ball radiation is negligible compared to the 6.53 watts dissipation rate. The effect of different ball surface emissivity on film temperature should therefore be negligible.

## APPENDIX B

Relative Contribution of Sapphire Radiance

As an order of magnitude approximation it has been assumed that the upper sapphire surface is at ambient temperature (25°C) and that the lower surface is at a temperature equal to that of the average fluid temperature (115°C). These temperatures correspond to black body radiance values of  $3.7 \times 10^{-3}$  and  $40 \times 10^{-3}$  watts/cm<sup>2</sup> -ster respectively. This data represents the maximum temperature condition on the contact centerline. The radiance characteristic of the sapphire should be less than the average of the surface radiance values, due to the fourth power relation between temperature and radiance. For an average black body radiance of  $22 \times 10^{-3}$  watts/cm<sup>2</sup> -ster and a sapphire emissivity of 0.018, the sapphire radiance becomes  $0.4 \times 10^{-3}$  watts/cm<sup>2</sup> -ster, which 2% of the black body ball radiance shown in equation (16). The 2% maximum error resulting from omitting the contribution from the sapphire will result in an error in ball temperature of less than 2°C.

## REFERENCES

- [1] T. E. Tallian - Electrohydrodynamic Hertzian Contacts, Part 1  
Nov. 1971 - Mechanical Engineering, page 14-18.
- [2] T. E. Tallian - Electrohydrodynamic Hertzian Contacts, Part 2  
Dec. 1971 - Mechanical Engineering, pag. 17-22.
- [3] Martin, H. M. (1916), Lubrication of Gear Teeth, Engineering,  
Lond., 102, 199.
- [4] Hamilton, G. M. and Moore, S. L., "Deformation and Pressure  
in an Elastohydrodynamic Contact", Proc. Royal Society Lond.,  
322A, 1971, pp. 313-330.
- [5] Dowson, D. and Longfield, M.D., The Distribution of Pressure  
and Temperature in a Highly Loaded Lubricated Contact, Inst.  
Mech. Engrs. Lubrication and Wear Convection.
- [6] Dowson, D. and Higginson, G.R., Stress Distribution in Lubri-  
cant Rolling Contacts - Proc. Symp. on Fatigue Contact.  
Paper 6,66 - Inst. Mech. Eng. - London.
- [7] Grubin, A. N. and Vinogradova, I.E., Central Scientific  
Research Institute of Technology and Mechanical Engineering,  
Book No. 30, Moscow. (DSIR Translation No. 337).
- [8] Robert C. Juvinall - Stresses, Strain and Strength, McGraw-  
Hill Book Co. pg. 370-397.
- [9] Nieman, G. and Gartner, F. Distribution of Hydrodynamic Pres-  
sure on Counterformal Line Contacts, A.S.L.E. Paper No. 64 LC-  
12, Presented to the joint A.S.M.E.-A.S.L.E. International  
Conference, Washington, D. C. 13-16 Oct. 1964.
- [10] Kannel, J. W., Bell, J. C. and Allen, C. M. Methods for  
Determining Pressure Distribution in Lubricated Rolling  
Contacts, A.S.L.E. Paper No. 64 LC-24 Presented to the joint  
ASME-ASLE International Lubrication Conference, Washington,  
D.C. 13-16 Oct. 1964.

- [11] Sanborn, D.M., and Winer, W. O., "Fluid Rheological Effects in Sliding Elastohydrodynamic Point Contacts with Transient loading: 1 - Film Thickness", Trans. ASME, Journal of Lubrication Technology, vol. 93, pp. 262-271, 1971.
- [12] Sanborn, D. M., and Winer, W.O., "Fluid Rheological Effects in Sliding Elastohydrodynamic Point Contacts with Transient Loading: 11 - Traction", Trans. ASME, Journal of Lubrication Technology, vol. 93, pp. 342-348, 1971.
- [13] Blok, H. "General Discussion on Lubrication", Vol.II,1. Mech.E., London, 1937, p. 14.
- [14] Crook, A. W., "The Lubrication of Rollers,-II, IIF", Phil. Trans. Roy. Soc. London, Series A, 1961, vol. 254, p. 223.
- [15] Cheng, H. S. and Sternlicht, B., "A Numerical Solution for the Pressure, Temperature and Film Thickness Between Two Infinitely Long, Lubricated Rolling and Sliding Cylinders Under Heavy Load", Trans. ASME, J. Basic Eng., vol. 87, 1965, pp. 695-707.
- [16] Dowson, D. & Whittaker, A. V., "A Numerical Procedure for the Solution of the Elastohydrodynamic Problem of Rolling and Sliding Contacts Lubricated by a Newtonian Fluid", Proc. I. Mech. E., vol. 180, Pt. 3B, 1965-66, pp. 57-71.
- [17] Archard, J. F., "The Temperature of Rubbing Surfaces", Wear Vol. 2, No. 6, p. 438, 1959.
- [18] Wolveridge, P. E., and Archard, J. F., "Temperature Distributions in Elastohydrodynamic Films: a New Analytic Solution", I. Mech. E., Tribology Meeting, 1972 (to be published).
- [19] Cheng, H. S., and Orcutt, F. K., "A Correlation Between the Theoretical and Experimental Results on the Elastohydrodynamic Lubrication of Rolling and Sliding Contacts", Proc. I. Mech.E., vol. 180, pt. 3B, 1965-66 pp. 158-168.
- [20] Kebler, R. W., "Optical Properties of Synthetic Sapphire", Linde Company, 30 East 42nd St., New York, New York.

- [21] McMahon, H. O., "Thermal Radiation From Partially Transparent Reflecting Bodies", Journal of the Optical Society of America vol. 40, No. 6, pp. 376-380, 1950.
- [22] Kreith, F., Principles of Heat Transfer, International Textbook Company, pp. 177-180, 1964.
- [23] Sanborn, D. M., An Experimental Investigation of the Elastohydrodynamic Lubrication of Point Contacts in Pure Sliding, Ph.D. Dissertation, University of Michigan, Dec. 1969 and University Microfilms, Inc., Ann Arbor, Michigan.
- [24] Winer, W. O., and Novak, J. D., "Some Measurements of High Pressure Lubricant Rheology", Journal of Lubricant Technology, Trans. ASME, Series F, Vol. 90, No. 3, July 1968, pp. 580-591.
- [25] Jacobsen, J., Lubricant Rheology at High Shear Stress, Ph.D. Dissertation, Georgia Institute of Technology, 1973 (to be completed).